A FINITE VOLUME TRANSIENT GROUNDWATER FLOW MODEL

By

Nathan Muyinda
BSc.Educ(Mak), PGD(AIMS), MC(MRI)
2011/HD13/2833U

A Dissertation Submitted to the Directorate of Research and Graduate Training in Partial Fulfilment of the Requirements for the Award of Master of Science in Mathematical Modelling of Makerere University

May 2014

Declaration

I Nathan Muyinda declare that this dissertation is my own work and to the best of my knowledge, no part of it has been submitted for any award in any university or institution of higher learning.

Signature.....

Date.....
Nathan Muyinda
Reg No. 2011/HD13/2833U

Approval

This dissertation has been submitted for examination with the approval of the following supervisors.

Signature.....

Date:.....
Dr. G. Kakuba, PhD
Department of Mathematics,
Makerere University.

Signature.....

Date:.....
Dr. J.M. Mango, PhD
Department of Mathematics
Makerere University

Dedication

This dissertation is dedicated to my dear parents; James Kamulegeya and Sarah Nakityo. It is also a dedication to my beloved sisters Suzan, Lilian, Molly and Joan and my brother Derrick.

Acknowledgement

I would like to express my gratitude to all those who gave me the possibility to complete this dissertation. I want to thank the Eastern Africa Universities Mathematics Programme (EAUMP) for awarding me the scholarship to pursue this masters programme for the full two years. I am extremely grateful to Dr. Juma Kasozi, Head of Mathematics Department and Coordinator EAUMP, Makerere University, for ensuring that I got the EAUMP scholarship. This dissertation would not be realised without his help.

I am deeply indebted to my supervisors Dr. John Mango and Dr. Godwin Kakuba whose help, suggestions and encouragement helped me in all the time of research for and writing of this dissertation. In a special way, I thank Dr. J. M. Mango for giving me that chance to participate in the Centre for International Mobility (CIMO) exchange programme at Lappeenranta University of Technology in Finland. The time spent there gave me invaluable access to most of the literature needed to write this dissertation.

My Colleagues in the Department of Mathematics, Makerere University, supported me in my research work. I want to thank them all for their help. I thank Mr. M. K. Nganda for always having the time to listen when I tell him about my work, Mr. I. Ndikubwayo for the fun and jokes and everyone in the department for the love fun during the lunchtime breaks. I am very grateful.

Contents

List of Figures

Abstract

In Kampala, groundwater is the major water source for about 50% of the population. An understanding, therefore, of the groundwater flow patterns is of absolute importance. In this work, we have described an isotropic transient groundwater flow model using parameter values obtained from Bwaise III, a Kampala suburb. An orthogonal grid finite volume method with quadrilateral control volumes has been used to simulate the model using mixed boundary conditions. We observed that a steady state of the system is determined by the specified head boundary condition. The steady state is either approximately equal to the specified head boundary value or below the specified head boundary value depending on the amount of water flowing out of the system. By constructing a balance between inflow and outflow from the aquifer, we are able to maintain a steady amount of water in the system without the aquifer drying up.

Chapter 1

Introduction

1.1 Background

Groundwater is a term that is used to refer to all waters found beneath the earth's surface. Like surface water, groundwater is an extremely important component of the freshwater hydrologic cycle and constitutes about two thirds of the freshwater resources of the world, and, if the polar ice caps and glaciers are not considered, groundwater accounts for nearly all usable freshwater(Chapman, 1996). In many countries, agricultural, domestic and industrial water users rely on groundwater as a source of low-cost, high-quality water and as such the use and protection of groundwater resources is of fundamental importance to human life and economic activity.

In recent years, it has become apparent that many human activities can have a negative impact on both the quantity and quality of groundwater. Problems like over-pumping and contamination of the groundwater resource through waste disposal and other activities are occurring with increasing frequency. One way to objectively assess the impact of existing or proposed human activities on groundwater quantity and quality is through the use of mathematical models (Istok, 1989).

1.1.1 Groundwater and Aquifers

Groundwater is found in saturated layers called *aquifers* that lie under the surface of the earth (Spellman & Whiting, 2004). An aquifer is a geologic formation that can transmit, store and yield significant amounts of water. Aquifers are made up of a combination of solid

material such as rock and gravel , and open spaces called pores. They may be regarded as underground water storage reservoirs. Water enters the aquifer naturally through precipitation and influent streams and artificially through wells or other recharge methods. Water leaves the aquifer naturally through springs or effluent streams and artificially through pumping wells (Bear, 1972).

Aquifers may be classified as unconfined or confined depending upon the presence or absence of a water table (See Figures 1.1 and 1.2). A *water table*, also known as a *phreatic surface*, is the surface upon which the water pressure is equal to the atmospheric pressure. Below the water table is the zone of saturation where water pressures are greater than the atmospheric pressure and the pores are saturated with water. An *unconfined* or water-table aquifer is one in which a water table exists and serves as its upper boundary. Unconfined aquifers lie just under the earth's surface and are recharged from the ground surface above it. A *confined* aquifer, also known as a pressure aquifer or artesian aquifer, is one bounded above and below by impervious formations. The water in a confined aquifer is said to be under hydrostatic pressure.

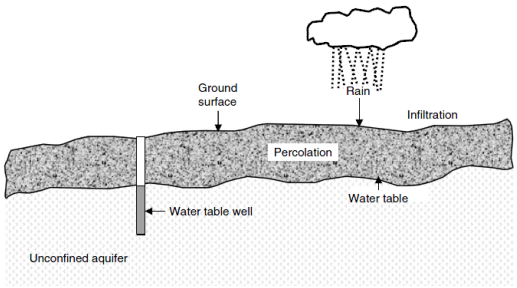

Figure 1.1: Unconfined aquifer (Spellman & Whiting, 2004)

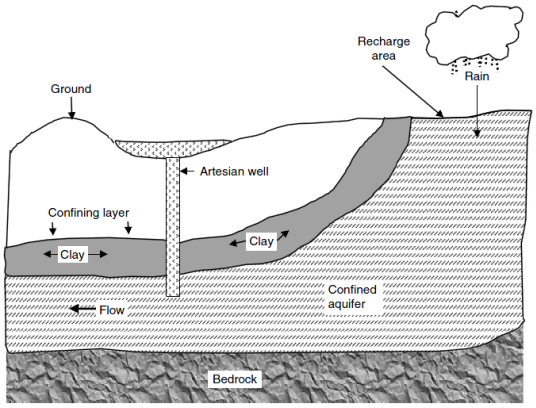

Figure 1.2: Confined aquifer (Spellman & Whiting, 2004)

Regardless of the type of aquifer, the groundwater in the aquifer is always in motion. The actual amount of water in an aquifer is dependent upon the amount of space available between the various grains of material that make up the aquifer. The amount of space is called the *porosity*. The ease of movement of water through an aquifer depends upon how well the pores are connected. The ability of an aquifer to pass water is called *Hydraulic conductivity*.

1.1.2 Aquifer Properties

The general properties of an aquifer to transmit, store and yield water are defined numerically through a number of aquifer parameters. We present here a brief general description of some of them.

(i) *Porosity* is defined as the ratio of the volume of voids (open spaces) to the total volume of material and is determined using the equation

$$n = \frac{V_{\text{void}}}{V_{\text{total}}}. \tag{1.1}$$

(ii) *Hydraulic Conductivity (K)* is defined as the ability of the aquifer material to conduct water through it under hydraulic gradients. It is a combined property of the porous medium and the fluid flowing through it. When the flow in the aquifer is horizontal, the term *Transmissivity (T)* is used and indicates the ability of the aquifer to transmit water through its entire thickness. It is the product of the hydraulic conductivity and the thickness of the aquifer,

$$T = Kb, \tag{1.2}$$

where b is aquifer thickness.

(iii) *Hydraulic head* (h) ; Groundwater moves in response to an energy gradient. The total energy available for groundwater flow is termed as the hydraulic head and consists of three components:

(a) Potential energy per unit weight also referred to as *elevation head*, z,

(b) *Pressure head*, $\frac{p}{\rho g}$, resulting from the pressure in the fluid, and

(c) Kinetic energy per unit weight also referred to as *velocity head*, $\frac{v^2}{2g}$, associated with the fluid's velocity.

Each of these terms is characterized by Bernoulli's equation

$$h = z + \frac{p}{\rho g} + \frac{v^2}{2g} \tag{1.3}$$

where g is acceleration due to gravity, z is the elevation of water mass above some datum level, p is the pressure, and ρ is the water density. In most cases of flow through

porous media, the kinetic energy head is much smaller than the pressure one, due to the very low velocity of the fluid (Bear & Cheng, 2010) and therefore the kinetic energy term can be safely dropped from the hydraulic head equation to obtain

$$h \approx z + \frac{p}{\rho g} \tag{1.4}$$

The hydraulic head at a point within an aquifer, expressed in equation (1.4), is measured using a device called a *piezometer* (or an observation well). It consists of a vertical pipe (or casing) inserted down to the point where the hydraulic (or piezometric) head measurement is required. The portion of the pipe that is located at the elevation at which this measurement is required, is slotted, perforated, or screened, and is often surrounded by a gravel pack to prevent clogging (see Figure 1.3). In this way, we enable a good hydraulic connection between the water in the well and water in the formation. The elevation of the water surface inside the well gives the hydraulic head at the location of the screen. A *hydraulic gradient* is the difference between hydraulic

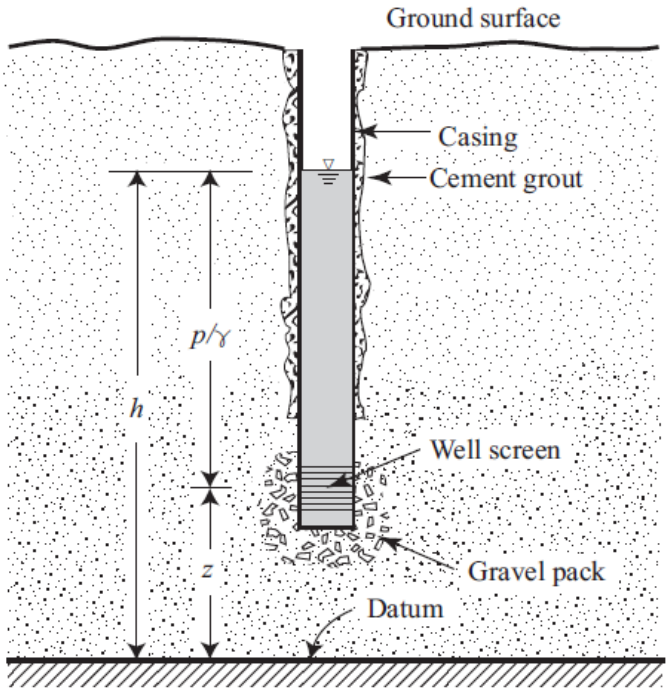

Figure 1.3: The hydraulic head measured in an observation well (Bear & Cheng, 2010).

heads measured at two points in an aquifer divided by the distance between them. By measuring the hydraulic heads at a number of spatially distributed observation wells tapping the same aquifer, a contour map can be drawn of a surface called the *piezo-*

metric surface. The elevation of this surface at a point in the horizontal plane gives the piezometric head in the aquifer at that point. In a given flow domain, the surface composed of all the points at which the hydraulic head has the same value is called an equipotential surface (Bear & Cheng, 2010).

(iv) *Specific Storage*(S_s) is defined as the volume of water produced by a unit volume of porous media during a unit decline of hydraulic head. The release of water from storage in a confined aquifer is due to compression of the solid matrix and decompression of the water and the specific storage, S_s, is given by (Gorelick, Freeze, Donohue, & Keely, 1993):

$$S_s = \rho g(\alpha + n\beta) \tag{1.5}$$

where α is the compressibility of the aquifer, β is the compressibility of water and n is aquifer porosity. When the flow in the aquifer is horizontal, the term *Storativity (S)* is used and is the product of the specific storage (S_y) and the aquifer thickness:

$$S = S_s b. \tag{1.6}$$

Storativity is defined as the volume of water released from a column of aquifer material of unit horizontal cross-sectional area per unit decline in hydraulic head. This quantity is sometimes called the coefficient of storage.

In unconfined aquifers, the release of water from storage is mainly due to the drainage of pore spaces and the storage coefficient is approximately the same as the percentage of pore space (porosity) of the aquifer. In such aquifers, neither specific storage nor storativity are appropriate terms for transient water-table aquifer problems. The *specific yield*, (S_y), is the storage parameter used and is defined as the volume of water released from storage per unit of horizontal cross-sectional area per unit decline in water-table elevation (Gorelick et al., 1993). S_y is much larger than S because the drainage porosity of an aquifer represents a much greater volume than that associated with compaction of the solid matrix and expansion of compressed water.

1.1.3 Groundwater Flow Equations

From the mathematical point of view, any mathematical model is based on formulating an equation (or a system of equations) that describe a phenomenon. Such equations are referred to as governing equations of the specified phenomenon. Governing equations are differential

equations that are derived from the physical principles governing the phenomenon that is to be modelled. In the case of groundwater flow, the governing equations are Darcy's law and the principle of mass balance (conservation).

1.1.4 Darcy's Law

In 1856, French engineer Henry Darcy while working on a project involving the use of sand to filter the water supply for the city of Dijon, France, performed laboratory experiments to examine the factors that govern the rate of flow of water through the sand (Fitts, 2002; Freeze, 1994). Through repeated experiments (See Figure 1.4), Darcy observed that the rate of flow, Q through a homogeneous sand column of uniform cross-sectional area was proportional to both the cross-sectional area of the column, A, and the difference in water level elevations, h_1 and h_2, at the inflow and outflow reservoirs of the column, respectively, and inversely proportional to the column length, L.

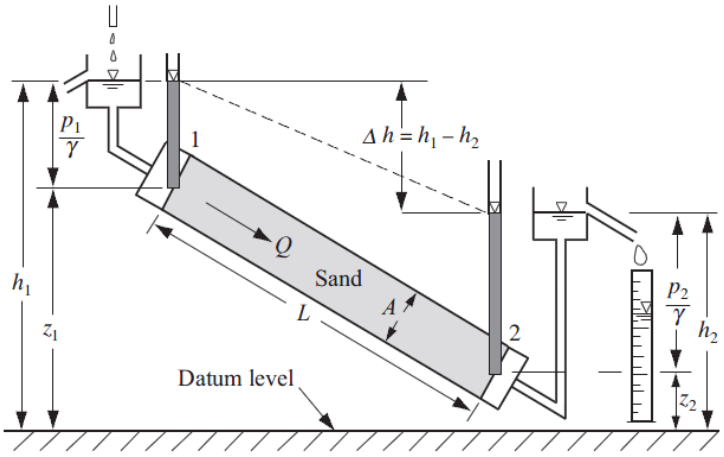

Figure 1.4: Experimental apparatus for the illustration of Darcy's Law (Bear & Cheng, 2010).

Combining these observations gives the basic empirical principle of groundwater flow in an equation now known as Darcy's law:

$$Q = KA\frac{h_1 - h_2}{L} \tag{1.7}$$

where K is the proportionality constant called the *hydraulic conductivity*.

Darcy's law (1.7) can also be expressed as the discharge per unit cross-sectional area as

follows:

$$q = \frac{Q}{A} = K\frac{h_1 - h_2}{L} \tag{1.8}$$

The quantity q is generally known as the *specific discharge* (or *Darcy flux* sometimes called the Darcy velocity).

Although, originally, Darcy's law in the form (1.7), or (1.8) was derived from experiments on a finite length column, Darcy's conclusion can be extended to what happens at a point along the column (Bear & Cheng, 2010). To achieve this, consider flow in a segment of a stream-tube in three-dimensional space aligned in a direction indicated by the unit vector **1s** (Fig. 1.5). The hydraulic head varies along the column, that is, $h = h(s)$. Consider a

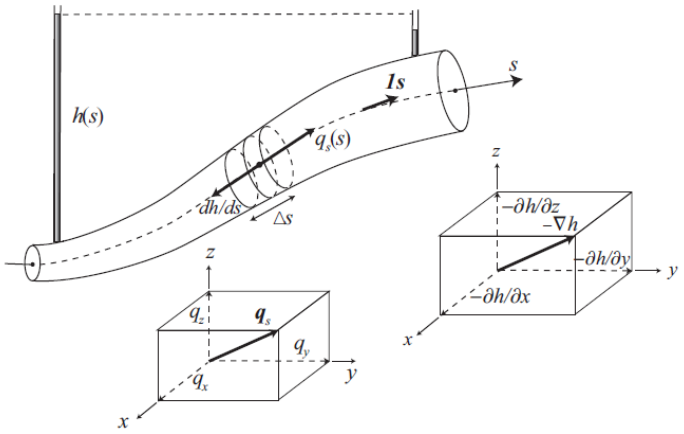

Figure 1.5: A stream-tube in three dimensional space (Bear & Cheng, 2010).

segment of this column of length Δs along the s-axis, between the coordinates $s - \frac{\Delta s}{2}$ and $s + \frac{\Delta s}{2}$. For this case, equation (1.8) takes the form:

$$q_s(s) = K\frac{h(s - \frac{\Delta s}{2}) - h(s + \frac{\Delta s}{2})}{\Delta s} \tag{1.9}$$

where the subscript s in q_s indicates that the flow is in the s-direction. Taking the limit as $\Delta s \to 0$ gives

$$\lim_{\Delta s \to 0} \frac{h(s - \frac{\Delta s}{2}) - h(s + \frac{\Delta s}{2})}{\Delta s} = -\frac{dh}{ds}, \tag{1.10}$$

and equation (1.9) reduces to

$$q_s = -K\frac{dh}{ds} \tag{1.11}$$

In this one-dimensional flow considered, the derivative $\frac{dh}{ds}$ is the slope of the hydraulic line, $h = h(s)$ and is referred to as the *hydraulic gradient*. The minus sign states that the flow takes place from a higher hydraulic head to a lower one, that is, hydraulic head decreases in the direction of flow. If there is flow in the positive s direction, q_s is positive and $\frac{dh}{ds}$ is negative. Conversely, when flow is in the negative s direction, q_s is negative and $\frac{dh}{ds}$ is positive.

It should be noted that Darcy's law (1.11), expressed in terms of the hydraulic head, h, is valid only for a fluid of constant density. When the fluid's density varies due to variations in pressure, concentration of dissolved matter, or temperature, the state variable to be used in the motion equation is pressure (Bear & Cheng, 2010).

In the real subsurface, groundwater flows in complex three-dimensional patterns. If we describe the geometry of the subsurface with a Cartesian xyz-coordinate system, there may be components of flow in each of these directions. Darcy's law for three-dimensional flow is analogous to the definition for one dimension (Zhang, 2011; Fitts, 2002):

$$\begin{aligned} q_x &= -K_x\frac{\partial h}{\partial x} \\ q_y &= -K_y\frac{\partial h}{\partial y} \\ q_z &= -K_z\frac{\partial h}{\partial z} \end{aligned} \tag{1.12}$$

where K_x, K_y and K_z are the hydraulic conductivity values in the x, y and z direction respectively. If the hydraulic conductivity is independent of the direction of measurement at a point in the porous medium, that is, $K_x = K_y = K_z$, the medium is called *isotropic* at that point. If the hydraulic conductivity varies with the direction of measurement at a point in a porous medium, that is, $K_x \neq K_y \neq K_z$, the medium is called *anisotropic* at that point. It should be noted that real geologic materials are never perfectly homogeneous (isotropic) but to ease calculations, it is often reasonable to assume that they are (Fitts, 2002).

In the generalized three-dimensional flow, the specific discharge, q, and the hydraulic gradient are all vector quantities (three components), the hydraulic head, h, is a scalar quantity (one component) and hydraulic conductivity, K, is a tensor quantity (nine components) (Fitts,

2002). Thus the generalized form of system (1.12) is written as:

$$\begin{aligned} q_x &= -K_{xx}\frac{\partial h}{\partial x} - K_{xy}\frac{\partial h}{\partial y} - K_{xz}\frac{\partial h}{\partial z} \\ q_y &= -K_{yx}\frac{\partial h}{\partial x} - K_{yy}\frac{\partial h}{\partial y} - K_{yz}\frac{\partial h}{\partial z} \\ q_z &= -K_{zx}\frac{\partial h}{\partial x} - K_{zy}\frac{\partial h}{\partial y} - K_{zz}\frac{\partial h}{\partial z} \end{aligned} \tag{1.13}$$

where K_{ij} may be interpreted as the contribution to the specific discharge in the ith direction, q_i, produced by a unit component of the hydraulic gradient in the jth direction (Bear & Cheng, 2010). When the axes of the xyz-coordinate system coincide with the principle axes of hydraulic conductivity (directions of maximum, minimum and intermediate K), then $K_{xy} = K_{xz} = K_{yx} = K_{yz} = K_{zx} = K_{zy} = 0$ and the form of Darcy's law given in equation (1.12) applies (Fitts, 2002). In practice, the more complex form of Darcy's law given in equation (1.13) is almost never needed and in this work, we shall also assume that the coordinate axes coincide with the principle axes and Darcy's law (1.12) shall be used in our calculations.

1.1.5 Equation of Mass Balance

One of the basic physical principles governing groundwater flow models is the law of mass conservation (balance). The law of mass conservation or continuity principle, states that *there can be no net change in the mass of a fluid contained in a small volume of an aquifer.* Any change in mass flowing into the small volume of the aquifer must be balanced by a corresponding change in mass flux out of the volume, or a change in the mass stored in the volume, or both.

Consider a very small part of the aquifer called a control volume having the shape of a rectangular parallel-piped box of dimensions $\Delta x, \Delta y, \Delta z$ centered at some point $P(x, y, z)$, Figure 1.6. At a certain instant, t, the mass of groundwater, M, present in the elementary control volume is given by

$$M = \rho\theta\Delta x\Delta y\Delta z \tag{1.14}$$

where θ is the volumetric fraction of water or moisture content of the porous medium, that is, volume of the fluid phase per unit volume of the control volume, and ρ is the density of the water. The quantity of water can change when groundwater enters or leaves the control

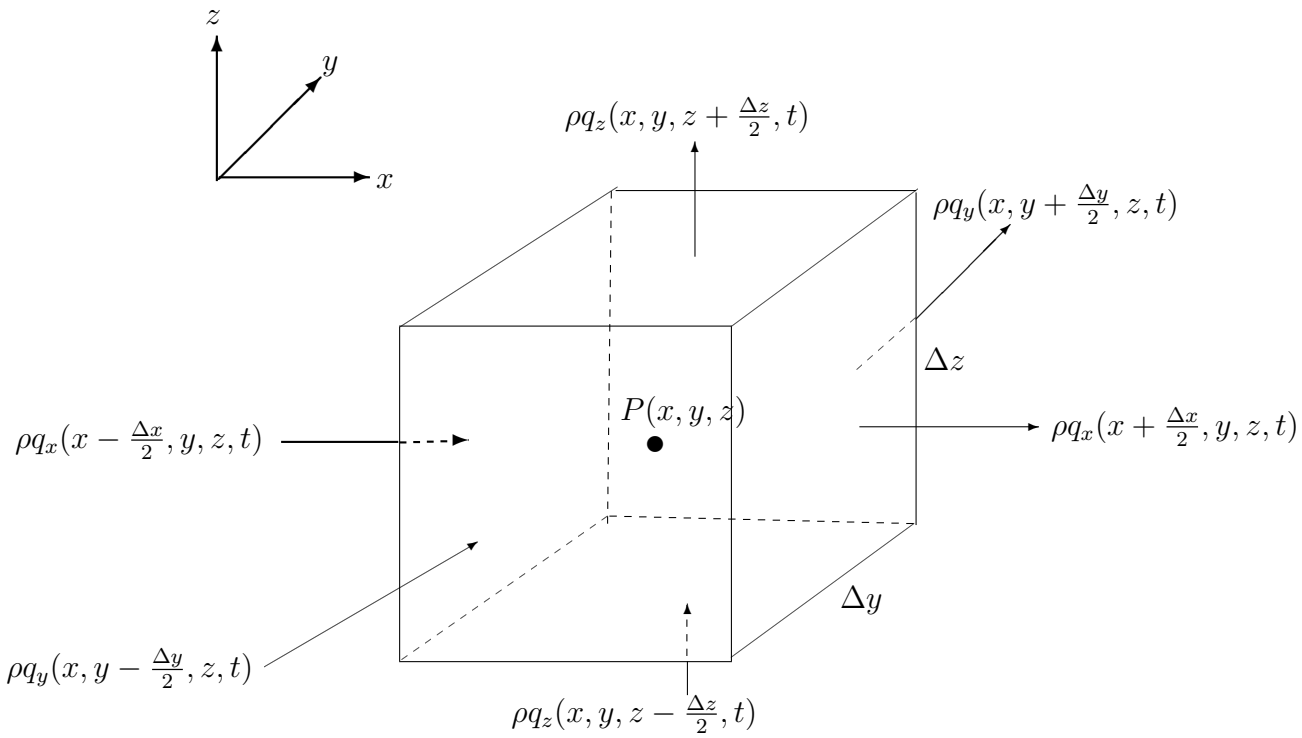

Figure 1.6: Mass conservation in an elementary control volume

volume through the sides. The principle of mass conservation states that the net result of inflow minus outflow is balanced by the change in storage, that is,

$$\frac{\partial M}{\partial t} = \text{inflow} \ - \ \text{outflow}, \tag{1.15}$$

hence it is necessary to calculate the groundwater flow through the sides of the control volume in order to evaluate the net result of inflow minus outflow.

Groundwater moves in only one direction through the control volume. However, the actual fluid motion can be subdivided on the basis of the components of flow parallel to the three principal axes. If q is the flux, which is the flow rate per unit cross-sectional area, ρq_x is the mass flux parallel to the x-axis, ρq_y is the mass flux parallel to the y-axis and ρq_z is the mass flux parallel to the z-axis. The mass of inflow of groundwater into the control volume along the x-axis is given by

$$\rho q_x(x - \frac{\Delta x}{2}, y, z, t)\Delta y \Delta z$$

and the mass of outflow from the control volume along the x-axis is

$$\rho q_x(x + \frac{\Delta x}{2}, y, z, t)\Delta y \Delta z.$$

For Δx small, q_x at position $x - \frac{\Delta x}{2}$ and $x + \frac{\Delta x}{2}$ can be approximated by a Taylor series expansion, where only zero and first-order terms are maintained such that the inflow and outflow along the x-axis are, respectively, given as

$$\left(\rho q_x - \frac{\Delta x}{2}\frac{\partial}{\partial x}(\rho q_x)\right)\Delta y \Delta z \text{ and } \left(\rho q_x + \frac{\Delta x}{2}\frac{\partial}{\partial x}(\rho q_x)\right)\Delta y \Delta z.$$

Hence the net accumulation of groundwater in the control volume due to movement parallel to the x-axis is equal to inflow minus outflow:

$$(\rho q_x - \frac{\Delta x}{2}\frac{\partial(\rho q_x)}{\partial x})\Delta y \Delta z - (\rho q_x + \frac{\Delta x}{2}\frac{\partial(\rho q_x)}{\partial x})\Delta y \Delta z = -\frac{\partial(\rho q_x)}{\partial x}\Delta x \Delta y \Delta z \tag{1.16}$$

Similar expressions can be obtained for the other two directions. Hence the net inflow over outflow in the control volume is given as

$$-\left(\frac{\partial \rho q_x}{\partial x} + \frac{\partial \rho q_y}{\partial y} + \frac{\partial \rho q_z}{\partial z}\right)\Delta x \Delta y \Delta z \tag{1.17}$$

Now from equation (1.14), the change in storage is given by

$$\frac{\partial M}{\partial t} = \frac{\partial}{\partial t}(\rho \theta \Delta x \Delta y \Delta z) \tag{1.18}$$

In the above expression, the variables that can really change with time are the water content, θ, because pores can be emptied or filled with water, the density of water, ρ, because water is compressible and the size of the control volume, $\Delta x \Delta y \Delta z$, because the porous medium can be compressible (Delleur, 1999). However, for the latter it is assumed that under natural conditions, only vertical deformation needs to be considered, such that only Δz depends upon time, while $\Delta x \Delta y$ remains constant. Hence equation (1.18) can be written as

$$\frac{\partial M}{\partial t} = \frac{\partial \rho}{\partial t}\theta \Delta x \Delta y \Delta z + \rho \frac{\partial \theta}{\partial t}\Delta x \Delta y \Delta z + \rho \theta \frac{\partial(\Delta x \Delta y \Delta z)}{\partial t} \tag{1.19}$$

In (Bear, 1972), it is shown that the compression of both water and the porous medium can be expressed as a function of the water pressure, that is,

$$\frac{\partial \Delta z}{\partial t} = \Delta z \alpha \frac{\partial p}{\partial t} \quad \text{and} \quad \frac{\partial \rho}{\partial t} = \rho \beta \frac{\partial p}{\partial t} \tag{1.20}$$

where α and β are the compressibility coefficients of the porous medium and water, respec-

tively, and p is the groundwater pressure. Substituting (1.20) into (1.19), we have

$$\frac{\partial M}{\partial t} = \rho \left[\theta(\alpha + \beta) \frac{\partial p}{\partial t} + \frac{\partial \theta}{\partial t} \right] \Delta x \Delta y \Delta z \tag{1.21}$$

The continuity equation is obtained by equating the change in storage given in equation (1.21) to the net inflow over outflow in the control volume given in equation (1.17). This gives the most general form of the mass balance equation as

$$-\left(\frac{\partial(\rho q_x)}{\partial x} + \frac{\partial(\rho q_y)}{\partial y} + \frac{\partial(\rho q_z)}{\partial z} \right) = \rho \left[\theta(\alpha + \beta) \frac{\partial p}{\partial t} + \frac{\partial \theta}{\partial t} \right] \tag{1.22}$$

which can also be written as

$$-\nabla \cdot (\rho \mathbf{q}) = \rho \left[\theta(\alpha + \beta) \frac{\partial p}{\partial t} + \frac{\partial \theta}{\partial t} \right] \tag{1.23}$$

where $\mathbf{q} = (q_x, q_y, q_z)$. In (McWhorter & Sunada, 1977), it is shown that

$$\nabla \cdot (\rho \mathbf{q}) \approx \rho (\nabla \cdot \mathbf{q}) \tag{1.24}$$

and the continuity equation (1.23) becomes

$$-\nabla \cdot \mathbf{q} = \theta(\alpha + \beta) \frac{\partial p}{\partial t} + \frac{\partial \theta}{\partial t} \tag{1.25}$$

This is the general mass balance (Continuity) equation expressing the change in storage of water in the control volume to the net inflow over outflow of water in the volume. In equation (1.25), α and β are the compressibility coefficients of the porous medium and water, respectively, p is the groundwater pressure, θ is the proportion of water (or moisture) in the porous medium control volume and $\mathbf{q}$ is the specific discharge vector.

1.1.6 General Flow Equation

The general groundwater flow equation is obtained by combining the continuity equation given in (1.25) with Darcy's law expressed in equation (1.12). This yields the following equation:

$$\nabla \cdot (\mathbf{K} \cdot \nabla h) = \theta(\alpha + \beta) \frac{\partial p}{\partial t} + \frac{\partial \theta}{\partial t} \tag{1.26}$$

where $\mathbf{K} = (K_x, K_y, K_z)$. From (Delleur, 1999), if groundwater density is assumed to be constant, the water pressure differences in time can be related to the temporal variation of the groundwater potential:

$$\frac{\partial p}{\partial t} = \rho g \frac{\partial h}{\partial t} \tag{1.27}$$

Thus, the groundwater flow equation (1.26) becomes

$$\nabla \cdot (\mathbf{K} \cdot \nabla h) = \rho g \theta (\alpha + \beta) \frac{\partial h}{\partial t} + \frac{\partial \theta}{\partial t} \tag{1.28}$$

This is the basic groundwater flow equation because it relates the amount of groundwater present, θ, and the groundwater potential, h, to the characteristics of the porous medium and the fluid in the space and time continuum.

By assuming that groundwater fully saturates the porous medium, the water content, θ, equals the porosity, n. That is, water content will be equal to the proportion of the material volume that is pore space. Under the assumption that the solid grains are incompressible, the porosity can be related to the compression of the porous medium, which depends on the water pressure or the groundwater potential, and it is shown in (Delleur, 1999) that

$$\frac{\partial \theta}{\partial t} = \frac{\partial n}{\partial t} = (1 - n)\alpha \frac{\partial p}{\partial t} = (1 - n)\alpha \rho g \frac{\partial h}{\partial t}. \tag{1.29}$$

Combining equations (1.28) and (1.29) and simplifying gives the general saturated transient groundwater flow equation for an anisotropic porous medium:

$$\nabla \cdot (\mathbf{K} \cdot \nabla h) = \rho g (\alpha + n\beta) \frac{\partial h}{\partial t} \tag{1.30}$$

Equation (1.30) can also be written as

$$\nabla \cdot (\mathbf{K} \cdot \nabla h) = S_s \frac{\partial h}{\partial t}, \tag{1.31}$$

where $S_s = \rho g(\alpha + n\beta)$ is the specific storage coefficient defined in equation (1.5).

Equation (1.31) is the most universal form of the saturated flow equation, allowing flow in all three directions, transient flow ($\frac{\partial h}{\partial t} \neq 0$), heterogeneous conductivities (for example $K_x = f(x)$) and anisotropic hydraulic conductivities. Other less general forms of the saturated flow equation can be derived from equation (1.31) by making the following simplifying assumptions:

(i) If the hydraulic conductivities are assumed to be homogeneous (K_x, K_y, K_z are independent of x, y, z), then,

$$\nabla \cdot (\mathbf{K} \cdot \nabla h) = \mathbf{K} \cdot \nabla^2 h$$

and the general equation (1.31) becomes

$$\mathbf{K} \cdot \nabla^2 h = S_s \frac{\partial h}{\partial t}. \tag{1.32}$$

This can be simplified further by making the assumption that the porous medium is homogeneous and isotropic, that is, $K_x = K_y = K_z = K$ and equation (1.32) becomes

$$\nabla^2 h = \frac{S_s}{K} \frac{\partial h}{\partial t} \tag{1.33}$$

(ii) If the flow is steady state ($\frac{\partial h}{\partial t} = 0$), the right-hand side of equations (1.31), (1.32) and (1.33) all become zero, that is,

$$\nabla \cdot (\mathbf{K} \cdot \nabla h) = 0 \tag{1.34}$$

$$\mathbf{K} \cdot \nabla^2 h = 0 \tag{1.35}$$

$$\nabla^2 h = 0 \tag{1.36}$$

Equation (1.36) is the famous Laplace equation that has a large number of applications in many branches of the physical and engineering sciences including fluid flow, heat conduction, electrostatics and so on. There exists a vast number of known solutions to the Laplace equation many of which apply directly to common groundwater flow conditions.

In many applications, groundwater is modelled as two-dimensional in the horizontal plane. This is because most aquifers have an aspect ratio like a thin pancake, with horizontal dimensions that are hundreds of times greater than their vertical thickness (Fitts, 2002). Also, the bulk of resistance encountered along a typical flow path is resistance to horizontal flow. Thus the groundwater hydrologist can assume the aquifer to be of constant thickness b and the flow to be horizontal (in the xy-plane). Hence the flow equation for an isotropic homogeneous porous medium is given as

$$\frac{\partial^2 h}{\partial x^2} + \frac{\partial^2 h}{\partial y^2} = \frac{S}{bK} \frac{\partial h}{\partial t}, \tag{1.37}$$

where $S = bS_s$ is the storativity (storage coefficient) of the aquifer. Since the product bK is

the transmissivity (see equation (1.2)), equation (1.37) is often written as

$$\frac{\partial^2 h}{\partial x^2} + \frac{\partial^2 h}{\partial y^2} = \frac{S}{T}\frac{\partial h}{\partial t}. \tag{1.38}$$

1.1.7 Flow Equation in Unconfined Aquifers

In an unconfined aquifer, the solution to the general flow equation (1.31) (whose RHS is, by the way, zero since $S_s = 0$) is complicated by the presence of a free surface water-table boundary condition. This is because as water is drawn from the aquifer through a well, for example, the position of the water-table around the well draws down forming a cone of depression. Thus the flow domain for which solutions of the general equation are sought is not constant because the water-table position changes with time. The fact that the water-table position is required (a priori) to define the flow domain in which equation (1.31) (with RHS= 0) applies and is also part of the required solution, makes an exact analytical solution very difficult to obtain (McWhorter & Sunada, 1977). An alternative formulation of the groundwater flow equation may be obtained by invoking the Dupuit assumption (or Dupuit-Forcheimer assumption).

1.1.8 The Dupuit-Forcheimer Approximation

Dupuit (1863) developed a theory based on a number of simplifying assumptions which are stated below:

(i) the hydraulic gradient is equal to the slope of the water table, and

(ii) for small water-table gradients, the flow is horizontal and the equipotential lines are vertical.

Figure 1.7 illustrates the difference between actual three-dimensional flow and flow modelled with the Dupuit-Forchheimer approximation.

To derive the governing equations for unconfined flow with Dupuit assumptions, we first do a continuity analysis for an infinitesimal slice of the aquifer (Figure 1.8). The slice is oriented perpendicular to the flow. The top of the representative volume is the water table and has height $h(x) = h_1$ at the left face and height $h(x) = h_2$ at the right face. The Dupuit assumption means that the slope of the water-table must be small. Because changes in water

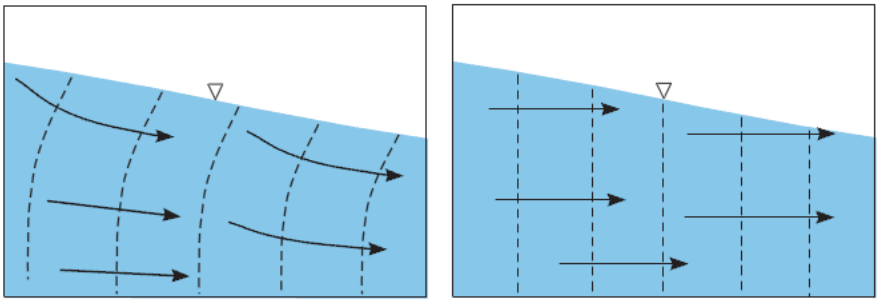

Figure 1.7: Cross-section of actual unconfined flow (left) and the same situation as modelled with the Dupuit-Forchheimer approximation (right). Hydraulic head contours are shown with dashed lines. In the Dupuit-Forchheimer model, there is no resistance to vertical flow, which results in constant head along the vertical lines ($\partial h/\partial z = 0$) (Zhang, 2011).

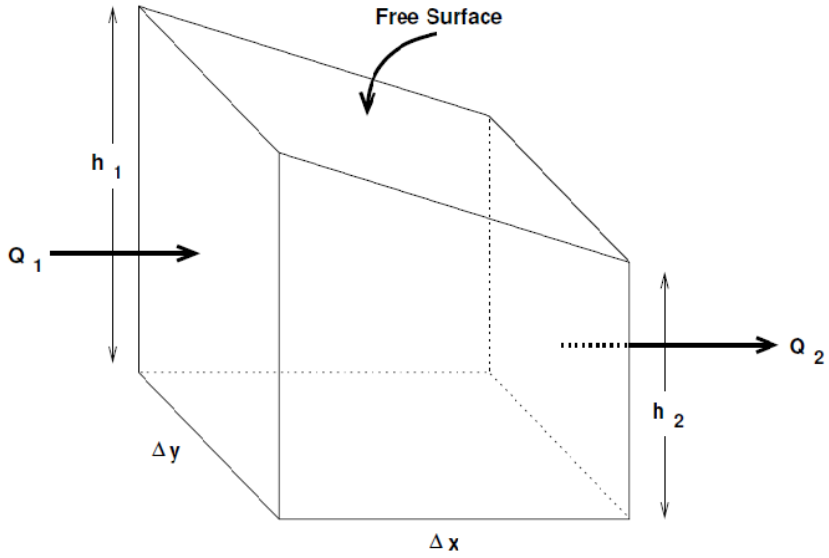

Figure 1.8: Infinitesimal volume of an unconfined aquifer. Top of the volume is the water table (free surface). Q_1 and Q_2 are volumetric rates of flow through this slice of the aquifer.

density are unimportant in unconfined aquifers, a volume balance, instead of a mass balance, is performed (McWhorter & Sunada, 1977).

Let Q_1 and Q_2 be the volumetric rates of flow through the left and right faces, respectively. By applying Darcy's law and multiplying by the area of each face, we have

$$Q_2 - Q_1 = \left(-K \left.\frac{dh}{dx}\right|_{x_2} \Delta y h_2\right) - \left(-K \left.\frac{dh}{dx}\right|_{x_1} \Delta y h_1\right) \tag{1.39}$$

Using the fact that

$$\frac{dh^2}{dx} = 2h\frac{dh}{dx}, \tag{1.40}$$

equation (1.39) can be written as

$$Q_2 - Q_1 = -\frac{K\Delta y}{2}\left(\left.\frac{dh^2}{dx}\right|_{x_2} - \left.\frac{dh^2}{dx}\right|_{x_1}\right) \tag{1.41}$$

If R is the recharge rate into the top of the representative volume, then a steady state volume balance is given by

$$Q_2 - Q_1 = R\Delta x\Delta y, \tag{1.42}$$

which when combined with equation (1.41) can be written as

$$-\frac{K}{2}\left[\frac{\left.\frac{dh^2}{dx}\right|_{x_2} - \left.\frac{dh^2}{dx}\right|_{x_1}}{\Delta x}\right] = R \tag{1.43}$$

Taking the limit as $\Delta x \to 0$, the steady one-dimensional unconfined flow under Dupuit assumptions is:

$$\frac{K}{2}\frac{d^2h^2}{dx^2} = -R \tag{1.44}$$

Hence the steady unconfined two-dimensional flow equation is given as:

$$\frac{K}{2}\left(\frac{\partial^2 h^2}{\partial x^2} + \frac{\partial^2 h^2}{\partial y^2}\right) = -R \quad \text{or} \quad \frac{\partial^2 h^2}{\partial x^2} + \frac{\partial^2 h^2}{\partial y^2} = -\frac{2R}{K} \tag{1.45}$$

For transient flow, the equation is given as:

$$\frac{\partial^2 h^2}{\partial x^2} + \frac{\partial^2 h^2}{\partial y^2} + \frac{2R}{K} = \frac{2S_y}{K}\frac{\partial h}{\partial t} \tag{1.46}$$

where S_y is the specific yield.

If there is no recharge/leakage, then $R = 0$ and the homogeneous unconfined aquifer flow equation is

$$\frac{\partial^2 h^2}{\partial x^2} + \frac{\partial^2 h^2}{\partial y^2} = \frac{2S_y}{K}\frac{\partial h}{\partial t} \tag{1.47}$$

Equation (1.47) is called the *nonlinear Boussinesq* equation. Equation (1.47) is nonlinear and thus difficult to solve by analytical methods. Linearization of the Boussinesq equation is permissible when the spatial variation of h remains small relative to h. In this case, it is possible to replace the variable saturated flow depth with an average thickness, b, and obtain

$$\frac{\partial^2 h}{\partial x^2} + \frac{\partial^2 h}{\partial y^2} = \frac{2S_y}{K}\frac{\partial h}{\partial t} \tag{1.48}$$

which is known as the *linearized Boussinesq* equation (McWhorter & Sunada, 1977).

1.2 Statement of the Problem

In Uganda, particularly Kampala, there are many unplanned, uncontrolled and growing urban settlements like Bwaise, Katanga, Makerere Kivulu and many more which lack elementary water and waste-handling services and this leads to a living enviroment that threatens the well-being of its inhabitants. Since groundwater-fed springs supply about 50% of Kampala's population, especially in these areas (Herzog, 2007), it is important to have a system that fully describes the groundwater flow pattern in these areas. In recent years mathematical models for simulating groundwater flow have become standard tools of the hydrologist. The reliability of model predictions is based on the ability of the mathematical model to adequately represent groundwater flow in the aquifer. For the groundwater fed springs in the areas mentioned above, there is no information of the underground water reservoirs and flows available. This study seeks to develop a transient mathematical groundwater flow model based on the finite volume method that can be used to estimate hydraulic heads and flow rates of the groundwater in the Bwaise settlement areas.

The governing equation for transient groundwater flow is:

$$\nabla \cdot \nabla h = \frac{S}{T}\frac{\partial h}{\partial t} \tag{1.49}$$

where h is the groundwater head, T is the transmissivity and S is the strorativity. Equation

(1.49) is solved on the domain Ω subject to the boundary and initial conditions:

$$h(\mathbf{x},t) = g_1(\mathbf{x},t), \;\; \mathbf{x} \in \partial\Omega_D \tag{1.50}$$

$$-\frac{\partial h}{\partial \mathbf{n}} = g_2(\mathbf{x},t), \;\; \mathbf{x} \in \partial\Omega_N \tag{1.51}$$

$$h(\mathbf{x},0) = f(\mathbf{x}), \;\; \mathbf{x} \in \Omega \tag{1.52}$$

where g_1 is prescribed head on $\partial\Omega_D$, g_2 is prescribed head gradient (flow) on $\partial\Omega_N$ in the direction of the the unit outward normal vector $\mathbf{n}$ of $\partial\Omega$ and f is the prescribed head at time $t = 0$.

Under the assumption of known aquifer parameters, the numerical solution of (1.49) by the finite volume method with the boundary and initial conditions (1.50), (1.51) and (1.52) leads to an equation system of the form:

$$\mathbf{A}_{N\times N}\mathbf{h}_N = \mathbf{b} \tag{1.53}$$

where $\mathbf{A}_{N\times N}$ is a symmetric N-square coefficient matrix, $\mathbf{h}_N$ is the vector of nodal heads and N is the number of nodes of the finite volume grid.

1.3 Objectives

Main objective

The main objective of this work is to develop a FVM simulation tool for groundwater flow modelling.

Specific objectives

The specific objectives of the study are to:

(i) describe the theory for groundwater flow models.

(ii) develop a groundwater flow model for Bwaise, a Kampala Suburb.

(iii) develop a FVM theory for a groundwater flow model.

(iv) write a MATLAB code for the FVM for an underground water flow model.

1.4 Significance of the Study

In Uganda, like other developing countries, sanitation and water supply are often inadequate. As a result, many low-income communities in these countries rely on untreated groundwater for drinking and other domestic use (Kulabako, 2005). In Kampala, 44% of the population live in unplanned and under serviced slums and of these only 17% have access to piped water and so springs are a major source of water for domestic use. Though spring water is considered to be aesthetically acceptable for domestic use, the presence of poorly designed pit latrines, poor liquid water management and soluble solid waste lead to contamination of water from the springs with pathogenic bacteria (Kulabako, 2005).

Previous studies on the groundwater situation in the peri-urban Kampala (Rukia, Ejobi, & Kabagambe, 2005; Kulabako, 2005) have looked at the water quality and pollution of the groundwater in these areas. This study develops a model based on the finite-volume technique that can be used by researchers and policy makers to predict groundwater flow rates and hence water supply in these areas by using local boundary conditions and area parameters in the simulations. It also aims to stimulate local research in the area of groundwater flow which is still low in the country and also to add on academic literature in the field.

1.5 Structure of the Dissertation

This dissertation consists of six chapters:

In Chapter 1, we described Darcy's Law and the Principle of Mass balance which are the founding principles of groundwater flow modelling and we were able to derive the differential equations governing the flow of water both in the steady and transient cases. We have also stated the objectives and significance of this work.

In Chapter 2, we review the literature on the use of numerical methods in groundwater flow and the available computer codes that have been developed.

In Chapter 3, we employed the transient mathematical model for Bwaise III parish developed by Herzog (2007) and, although the original model was not isotropic all over the study area, we averaged the hydraulic conductivities measured by Herzog and formed an isotropic groundwater flow model for the study area. Thus we used an isotropic transient groundwater flow model for Bwaise III to carry out our finite volume analysis.

In Chapter 4, we discuss in detail the finite difference method, the finite element method

and the finite volume method which are the three most frequently used numerical methods in the study of groundwater flow modelling.

In Chapter 5, we present an analysis and discussion of our results.

In Chapter 6, we give recommendations and conclusions.

Chapter 2

Literature Review

Numerical Modelling of groundwater is a relatively new field. It was not extensively pursued until the mid 1960s when digital computers with adequate capacity became readily available (Igboekwe & Achi, 2011). The digital computers provided the possibility of solving transient flow problems in complex geological systems, which are impossible to solve in closed form (analytic) solutions. The early numerical solutions were based on the finite-difference method and the method of relaxation, both of which were known before the advent of computers. Finite difference methods were relatively easy to use, but at the time they did not allow for a moveable water table boundary and this led to the development of finite-element methods.

Stallman(1956) introduced finite-difference method in groundwater literature. Much later, Nelson (1968) used the finite-difference method to study the inverse problem of groundwater. The finite-element method (Clough, 1960), which was initially developed in the aircraft industry to provide a refined solution for stress distributions in extremely complex airframe configurations, was employed by Zienkiewicz et al. (1966) to find steady-state solutions to heterogeneous and anisotropic flow problems and later to problems of transient flow in porous media(Iraj & Witherspoon, 1968).

Remson, Appel, and Webster (1965) helped popularize the computer modelling approach by developing a steady-state finite-difference computer model to predict the effects of a proposed surface water reservoir on the heads in an unconfined regional aquifer. They noted that one great advantage of the numerical method is that it was compatible with computer oriented methods of data storage and retrieval.

Freeze and Witherspoon (1966) described a finite difference numerical procedure for the solution of a steady-state groundwater flow in a three-dimensional, nonhomogeneous, anisotropic

aquifer and an analytical separation of variables technique restricted to the two-dimensional case. They concluded that the numerical method was more versatile and mathematically simpler of the two. In the numerical finite-difference method, the flow equation, which is a partial differential equation, is turned into a system of finite-difference equations with numerical values of flow parameters (e.g hydraulic conductivity) being supplied at finite points (or nodes) throughout the aquifer. Solution of this system of equations for the hydraulic head at each node permits determination of the direction and quantity of flow throughout the aquifer.

Pinder and Bredehoeft (1968) of the U.S. Geological Survey presented the first digital computer program for solving unsteady flow in a confined aquifer using an implicit finite-difference technique. In the same year, Kleinecke (1968) presented a finite difference groundwater simulation program called TELMA I and TELMA II capable of simulating groundwater flow in basins using an appropriate model of the basin as input data and concluded that simulation was the only practical way of utilizing present data and guide the development of better understanding of groundwater flows both for direct management purposes and as a means of improving geohydrological knowledge.

Prickett and Lonnquist (1971) at Illinois Geological Survey developed a popular finite-difference code called PLASM referred to as Pricket Lonnquist Aquifer Simulation Model, that could simulate one-, two- and three-dimensional transient flow in heterogeneous and anisotropic aquifer systems.

The development, documentation and availability of the two aquifer simulation programs by Pinder and Bredehoeft (1968) and Prickett and Lonnquist (1971) led to a boom in the use of computer simulation of aquifers in water resource evaluations in the 1970s:

- Freeze (1971) developed a three-dimensional finite-difference model for the treatment of saturated-unsaturated transient flow in small nonhomogeneous, anisotropic geologic basins. The model used the line successive over relaxation technique to solve the flow equation.

- Trescott (1975) and Trescott and Larson (1976) of the U.S. Geologiocal Survey developed a finite difference model for the simulation of groundwater flow in three dimensions. This model was later modified by Torak (1982) to extend it to simulations involving head-dependent sources and sinks and to enhance the iterative solution process of the strongly implicit procedure. The code was further developed and later became MODFLOW (McDonald and Harbaugh, 1988), the most popular and widely used groundwater simulation program.

- Reeves and Duguid (1975) developed a Galerkin finite-element computer program for the simulation of transient saturated-unsaturated groundwater flow in two dimensions where they used a backward difference scheme to approximate the time derivative $\frac{\partial h}{\partial t}$.

In the 1980's, research emphasis was to develop better computer models and to search for better numerical techniques to solve the governing nonlinear partial differential equations (PDEs). Advancements in computer technology eased the researchers' job and motivated them to attempt to solve more complex, challenging and time consuming groundwater flow problems. Parallel to these advancements, studies on numerical solution techniques increased rapidly. New numerical methods were developed and applied in models. The boundary integral equation method (Ligget & Liu, 1983), the analytic element method (Strack, 1989) and the finite volume method (Patankar, 1980; Rozon, 1989; Leveque, 2002) were relatively new techniques that were applied in models.

The finite-volume method, which is the basis of our work, was introduced by Patankar (1980). In his book, he developed the method for use in solving heat transfer and fluid flow problems. Today the finite-volume method is dominant throughout the field of computational fluid dynamics for solving the kind of PDEs encountered in this area. The major advantage of the method over the finite-difference and finite-element methods is that it is intimately connected to the underlying physical process. Most PDEs arise as a result of conservation of some physical quantity like mass, energy and momentum. In methods such as the finite-difference and finite-element, these quantities are not necessarily conserved at the discrete level, meaning that the approximate solutions may, owing to numerical error, exhibit physically unrealistic behaviour. The finite-volume method ensures that these quantities remain conserved, meaning that the method is in agreement with the underlying laws of physics at all levels of the discretisation (Patankar, 1980).

Another advantage of the method is its applicability to a variety of mesh structures and geometries. The formulation of the method lends itself to a very natural implementation of boundary conditions, even where the boundaries and associated boundary conditions are complicated. The mesh itself may be either structured or unstructured but the finite volume method works well with either.

From the late 1980s and throughout the 1990s, many sophisticated groundwater models were developed to deal with more challenging problems. The most well known of these was MODFLOW, created by McDonald and Harbaugh (1988), which is a three-dimensional finite-difference saturated groundwater flow model. It has a well organized modular structure that allows it to be modified easily to adapt the code for a particular application. Many new

capabilities have been added to the original 1988 model and it is still the most widely used groundwater modelling software to date.

Another popular groundwater simulation program is FEMWATER developed by Yeh et al. (1996). FEMWATER is a three-dimensional finite-element flow and contaminant transport model used to simulate both saturated and unsaturated conditions. It was formed by combining two older models, 3DFEMWATER (flow) and 3DLEWASTE (transport). FEMWATER was formed by combining the two codes into a single coupled flow and transport model. The 3DFEMWATER and 3DLEWASTE models were originally written by Yeh and Cheng (1994).

Research on the use of finite volume method in groundwater is ongoing and no simulation program is currently publicly available like in the case of finite difference and finite element methods. But many researchers have published work on the method: Loudyi, Falconer, and Lin (2007) developed a two dimensional finite-volume groundwater flow model using a cell-centered structured non-orthogonal quadrilateral grid and compared the results of the numerical model with analytical and results from a MODFLOW finite-difference model. They found that the use of the finite-volume method provides modellers with a consistent substitute for the finite difference methods with the same ease of use and an improved flexibility and accuracy in simulating irregular boundary geometries. In this work, we employ the finite volume method.

Chapter 3

The Model for Groundwater

3.1 Introduction

The groundwater resources of the earth have, for a long time, been subject to degradation as a result of man's increasing utilisation of natural resources and worldwide industrialisation. Beginning in the 1960s, contaminated aquifers were cleaned up and protected from further degradation in various countries around the world because government agencies identified groundwater as a valuable and increasingly important water resource (Batu, 2006). During this time, it was found that mathematical modelling for groundwater flow and solute transport could be used as an efficient and cost-effective tool in the investigation and management of groundwater resources. Since then, mathematical models of groundwater flow have been widely used for water supply studies and designing contaminant cleanup. The availability of computers and the development of efficient computer programs to do the computations involved in the models have also led to an increase in the use of numerical mathematical models in the analysis of groundwater flow and contaminant transport problems.

The Groundwater flow models are used to calculate the rate and direction of movement of groundwater through aquifers and confining units in the subsurface. These calculations are referred to as simulations. The outputs from the model simulations are the hydraulic heads and flow rates which are in equilibrium with the hydrogeological conditions (aquifer boundaries, initial and transient conditions and sources or sinks) defined for the modelled area.

3.2 Mathematical Modelling

A model is a tool designed to represent a simplified version of some more complex reality. It is created with the goal to gain new knowledge about the real world by investigating the properties and implications of the model. Mathematical models are conceptual descriptions or approximations that describe the physical system using mathematical equations. The reliability or usefulness of a model depends on how closely the mathematical equations approximate the physical system being modelled. In order to evaluate the applicability of a model, it is necessary to have a thorough understanding of the physical system and the assumptions embedded in the derivation of the mathematical equations. The equations are based on certain simplifying assumptions which involve; in this case, direction of flow, geometry of the aquifer, heterogeneity or anisotropy of sediments within the aquifer and other physical properties of the aquifer. Due to these assumptions and the many uncertainties in the data values required by the model, a model must be viewed as an approximation and not an exact duplication of field conditions.

The modelling process is a series of steps that involves collecting and reviewing all the available data about the material properties, heads and discharges in the vicinity of the region to be modelled and converting this into a conceptual model. A conceptual model is a descriptive representation of a groundwater system that incorporates an interpretation of the geological and hydrological conditions. A good conceptual model should describe the reality in a simple way that satisfies modelling objectives and management requirements. It should summarize our understanding of water flow or contaminant transport. The key issues that the conceptual model should include are (König & Weiss, 2009):

(i) Aquifer geometry and model domain

(ii) Boundary conditions

(iii) Aquifer parameters like hydraulic conductivity, porosity, storativity, etc

(iv) Groundwater recharge

(v) Water balance

Once the conceptual model is built, the mathematical model can be set up. The mathematical model represents the conceptual model and the assumptions made in the form of differential equations that can be solved either analytically or numerically. The modelling methodology is summarised in Figure 3.1.

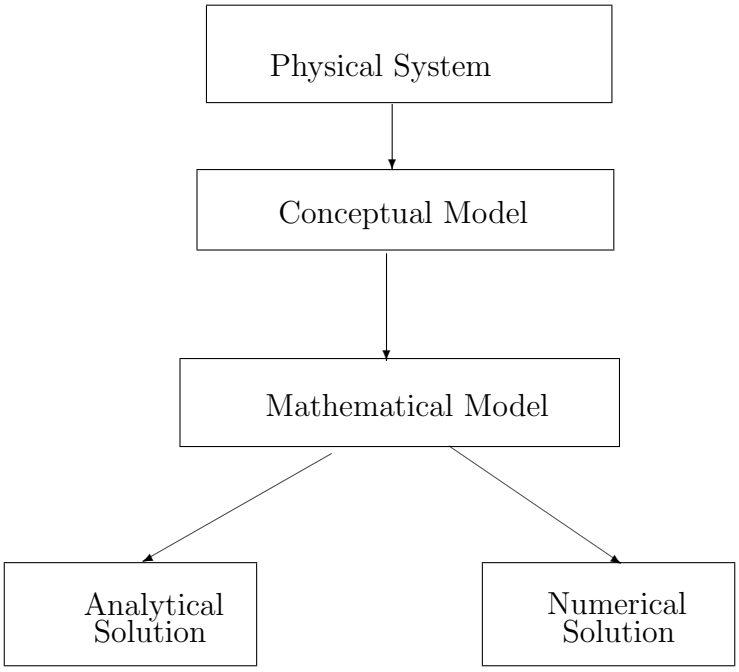

Figure 3.1: Modelling methodology

3.3 Boundary and Initial Conditions

To obtain a unique solution of the partial differential equations for a groundwater model, additional information about the physical state of the system is required. This information is supplied by boundary and initial conditions. For steady-state problems, only boundary conditions are required, whereas for transient problems, both boundary and initial conditions must be specified. Improper specification of boundary and initial conditions affects the solution and may result in a completely incorrect output.

3.3.1 Boundary Conditions

In groundwater investigations, the system under study should ideally be enclosed by a boundary surface that corresponds to identifiable hydro-geologic features at which some characteristic of groundwater flow is easily described. Examples include a body of surface water, an almost impermeable surface, a water table and a drain channel.

Specifying the boundary conditions of the groundwater flow system means assigning a boundary type, usually one or a combination of the types listed below to every point on the boundary surface. The boundary conditions include the geometry of the aquifer body and

the value of the dependent variable or its derivative normal to the boundary. The selection of the boundary surface and boundary conditions is one of the most critical step in conceptualizing and developing a model of a groundwater system (Lehn O. Franke & Bennett, 1984). The principal types of boundary conditions include:

(i) Specified-head boundary (Dirichlet conditions): This occurs wherever head can be specified as a function of position and time over part of the boundary surface of a groundwater system. An example of the simplest type might be an aquifer that is exposed along the bottom of a large stream whose stage is independent of groundwater seepage. As one moves upstream or downstream, the head changes in relation to the slope of the stream channel. If changes in head with time are insignificant, the head can be specified as a function of position alone ($h = f(x, y)$) at all points along the stream bed. When the stream stage varies with time, the head at points along the stream bed would be specified as a function of both position and time, $h = f(x, y, t)$.

In both cases, heads along the stream bed are specified according to conditions external to the groundwater system and maintain these values throughout the problem solution, regardless of the stresses to which the groundwater system is subjected.

(ii) Specified flux boundary (Neumann conditions): This occurs wherever the flux (volume of fluid per unit time per unit cross-sectional area) across a given part of the boundary surface can be specified as a function of position and time. In the simplest type of specified flux boundary, the flux across a given part of the boundary is considered uniform in space and constant in time. An example is areal recharge crossing the upper surface of an aquifer. Boundaries of this type are called constant flux boundaries. In a more general case, the flux might be constant with time but specified as a function of position: $q = f(x, y)$ over the part of the boundary surface in question. In the most general case, flux is specified as a function of time as well as position $q = f(x, y, t)$.

In all the three cases, flux across the boundary is specified in advance and not affected by events within the groundwater system; moreover, it may not deviate from its specified values during the problem solution.

For an isotropic medium, the flux from the boundary into an aquifer is given by Darcy's law as $q = -K\dfrac{\partial h}{\partial n}$ where q is the specific discharge , K the hydraulic conductivity, h is the hydraulic head and n is the direction normal to the boundary. For the constant-flux boundary we have $\dfrac{\partial h}{\partial n}$ = constant, and for the two more general cases, we have $\dfrac{\partial h}{\partial n} = f(x, y)$ and $\dfrac{\partial h}{\partial n} = f(x, y, t)$, respectively.

Real problems have mixed boundary conditions, a combination of Dirichlet and Neuman conditions. It is called the boundary condition of the third kind. It is necessary sometimes to approximate boundary conditions to limit the region of the problem domain (Wang & Anderson, 1982). If inconsistent or incomplete boundary conditions are specified, the problem itself is ill defined.

3.3.2 Initial Conditions

Defining a specific groundwater flow problem always involves specification of boundary conditions, and in transient-state problems, the initial conditions must be specified as well. Definition of initial conditions means specifying the head distribution throughout the system at some particular time. These specified heads can be considered as reference heads. Calculated changes in head through time will be relative to these given heads and the time represented by these reference heads becomes the reference time. As a convenience, this reference time is usually specified as zero, and the time frame is reckoned from this initial time.

In more formal terms, an initial condition gives the head as a function of position at $t = 0$, that is,

$$h = f(x, y; t = 0).$$

This notation suggests that initial conditions are boundary conditions in time. The initial conditions are simply the values of the dependent variable specified everywhere inside the boundary at the start of the simulation.

3.4 Problem Model

We shall consider the second-order transient groundwater flow equation

$$\nabla \cdot \nabla h = \frac{S}{T} \frac{\partial h}{\partial t} \tag{3.1}$$

and carry out a finite-volume simulation of the problem based on the boundary and initial conditions from Herzog (2007) for Bwaise III parish in Kawempe Division, Kampala District. From Herzog (2007), the study area is bordered to the north by Nabweru road, to the east by Bombo road, to the south by the Bwaise-Nsooba drainage channel and the west by the Nakamiro drainage channel as shown in Figure 3.2.

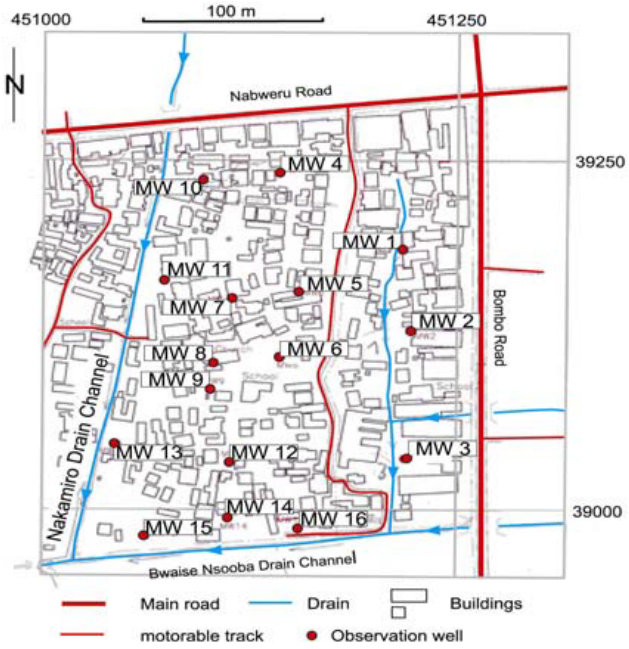

Figure 3.2: Bwaise III study area.It is 6.65 ha large (Herzog, 2007).

According to Herzog (2007), the aquifer was divided into two layers: top layer A and bottom layer B and the hydraulic conductivity varies remarkably in the study area because of area building. The conductivity of the first layer is shown in Fig. 3.3 and the value for layer B was set to 0.017m/d (meters per day). The bottom of the aquifer was defined as impermeable. The aquifer has a depth of 15m meeting the bedrock that is impermeable. A simplified cross-section illustrating the groundwater flow system is shown in Figure 3.4.

According to Herzog (2007), the main flow enters the system from the eastern and northern borders. The groundwater leaves the system in western and southern directions. This assumption is supported by the direction of flow of flood surface water after rainfall events. Since the northern and eastern sides of the study area experience inflow, the arcs delineating those boundaries were assigned to be specified head arcs. Specified head boundary conditions make it possible to adjust the head at the boundary. In the first attempt to create a simulation, the specified head was set at 5m below the ground surface, uniformly along the boundary. The head is assigned at the nodes and varies linearly over the connecting arc.

The drainage channels that form the western and southern boundaries will act as sinks, i.e. remove water from the aquifer, as long as the groundwater table is above the elevation of the drain. The drain will have no effect if the groundwater level falls below the bottom elevation of the drain. The rate of flow from the aquifer to the drain is proportional to the

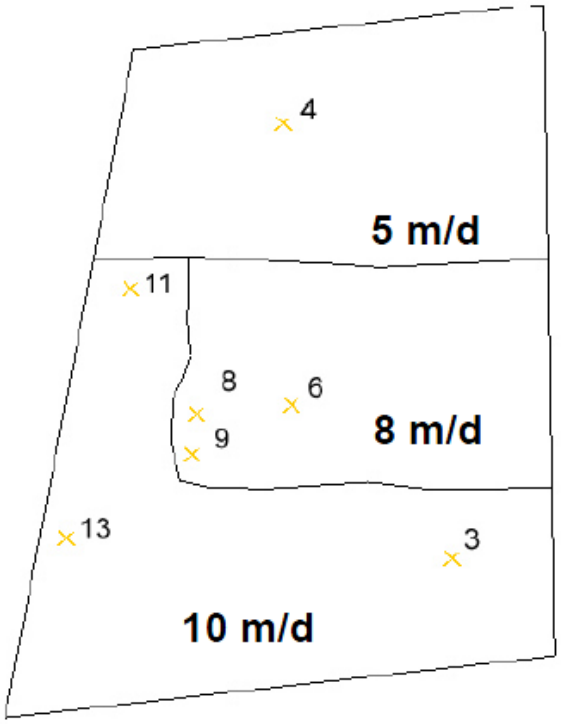

Figure 3.3: Subdivision of the study area with similar hydraulic conductivities of the top layer (Herzog, 2007)

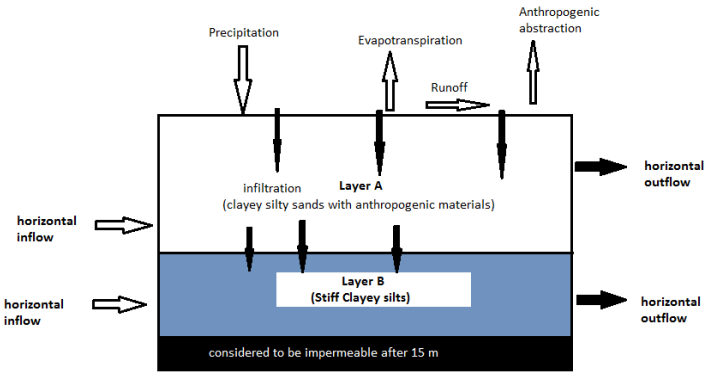

Figure 3.4: An idealized cross-section of the study area, with flow system (Herzog, 2007)

difference in height between the groundwater table and the drain bottom. The constant of this proportionality is the conductance of the fill material surrounding the drain.

In the wet season, the runoff drainage channels tend to flow full, with the water levels exceeding the groundwater table. Thus in the wet months, the conductance of the drain is set very low, to simulate the absence of flow from the groundwater into the drain. This ensures that groundwater does not flow into the drain considering that flow from the drain

into the groundwater is most likely.

In this work, we shall assume an isotropic study area with hydraulic conductivity K given by the average value of the hydraulic conductivity of the two layers. Thus the parameters for Bwaise III study area to be used for our simulation are (Thunvik, 2010):

$$K = \frac{5 + 8 + 10 + 0.017}{4} = 5.75\text{m/d} = 3.99 \times 10^{-3}\text{m/s},$$

$n = 0.56, \alpha = 10^{-5}$ ms^2/kg, $\beta = 4 \times 10^{-4}$ms^2/kg, $\rho = 1000$kg/m^3 and $g = 9.8$m/s^2 and aquifer thickness $b = 15$m. Thus the specific storage coefficient S_s is given as

$$S_s = \rho g(\alpha + n\beta) = 9.8 \times 1000 \times (10^{-5} + 0.56 \times (4 \times 10^{-4})) = 2.2947\text{m}^{-2} \tag{3.2}$$

The Storativity S is given as

$$S = bS_s = 15 \times 2.2947 = 34.4205\text{m}^{-1} \tag{3.3}$$

and the transmissivity T,

$$T = Kb = 3.99 \times 10^{-3} \times 15 = 0.05985\text{m}^2\text{s}^{-1} \tag{3.4}$$

Thus we are going to carry out a finite volume simulation using quadrilateral control volumes and orthogonal mesh of the problem:

$$\nabla \cdot \nabla h = \frac{S}{T}\frac{\partial h}{\partial t}, \;\; (x, y) \in [0, 300] \times [0, 300], \; t \geq 0 \tag{3.5}$$

with boundary and initial conditions:

$$\begin{aligned} h(300, y, t) = h(x, 300, t) &= 12 \\ \mathbf{n} \cdot \nabla h = 0; \;\; x = 0, y &= 0 \\ h(x, y, 0) &= 10 \end{aligned} \tag{3.6}$$

where $\mathbf{n}$ is the outward unit normal to the boundary.

This model describes transient flow in a two-dimensional homogeneous isotropic confined aquifer of constant thickness b as shown in Figure 3.5.

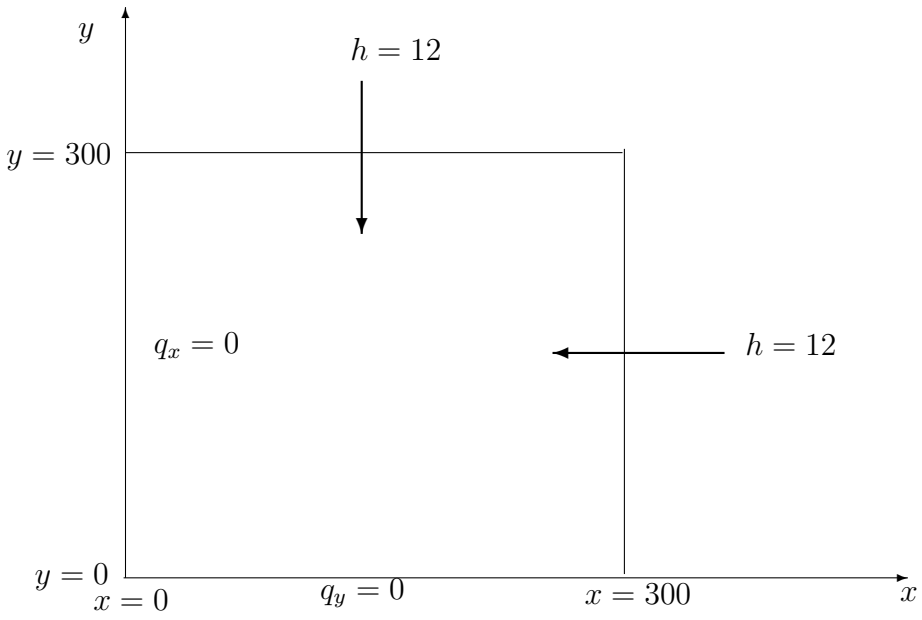

Figure 3.5: Model domain and boundary conditions.

Chapter 4

Solution Methods

4.1 Analytical Solutions

An analytic solution seeks to determine the spatial and temporal distribution of the model's state variable, that is, $h = h(x, y, t)$, as a continuous function of space and time. Analytical solutions are available only for simplified groundwater flow and contaminant transport problems. For example, many analytical solutions require that the medium be homogeneous and isotropic. The advantages of an analytical solution, when it is possible to apply one, are that it provides a continuous and exact solution to the governing equation and is often relatively simple and efficient to use (Delleur, 1999; König & Weiss, 2009).

As an example, consider a one-dimensional transient flow in a homogeneous porous medium of finite length, with specified head boundary conditions on each end of the domain, governed by the equation(Pinder & Celia, 2006):

$$\begin{aligned} S_s \frac{\partial h}{\partial t} - K \frac{\partial^2 h}{\partial x^2} =& 0, \quad 0 < x < l, t > 0, \\ h(0,t) =& h_L(t) = h_L = \text{constant}, \\ h(l,t) =& h_R(t) = 0, \\ h(x,0) =& h_{\text{init}}(x) = 0. \end{aligned} \tag{4.1}$$

Solving this equation by the method of separation of variables, the solution is given as

(Pinder & Celia, 2006),

$$h(x,t) = \frac{2}{\pi}\sum_{n=1}^{\infty}\frac{h_L}{n}sin\left(\frac{n\pi x}{l}\right)\left[1-\exp\left(-\frac{kn^2\pi^2 t}{S_s l^2}\right)\right]. \tag{4.2}$$

Analytical solutions for groundwater flow problems in more than one dimension become more complicated because the governing equation is a partial differential equation (PDE) rather than an ordinary differential equation (ODE). ODEs typically have finite-dimensional solution spaces. The solution may be written as a linear combination of a finite number of fundamental solutions. PDEs usually have infinite-dimensional solution spaces and the solutions involve infinite series and/or various kinds of integrals (Pinder & Celia, 2006), such as the one in equation (4.2).

For simulating most field problems, the mathematical benefits of obtaining an exact analytical solution are probably outweighed by the errors introduced by the simplifying assumptions about the complex field environment that are required to apply the analytical approach (Delleur, 1999). To deal with more realistic situations, it is usually necessary to solve the mathematical model approximately using numerical techniques. In this work we will use numerical solutions.

4.2 Numerical Solutions

Since the 1960s when high-speed digital computers became widely available, numerical simulation methods have gained importance in the study of groundwater flow, management or the spreading of contaminants in subsurface systems. A numerical solution seeks to determine the spatial temporal distribution of the model's state variables only at a selected set of points in space and time. Information on what happens at all other points of interest is obtained by interpolation. In this way, the problem is transformed from one described by a continuous mathematical model, written in terms of a small number of variables which are continuous functions of space and time, that is, $h = h(x, y, t)$, to one described by a discrete mathematical model, written in terms of many discrete values of these variables defined at specified points in space and time (Bear & Cheng, 2010), that is, h_i^m, for h at a point in space marked as i and a time level marked as m.

The small number of PDEs that contain the continuous variables is replaced by a large number of linear algebraic equations that contain the discrete variables. This system of algebraic equations can then be solved by, for example, using matrix techniques or using

a computer code. Once these discrete values are solved for, we can obtain information on what happens at every point in the space and time domains of interest by appropriate interpolation. The most widely used numerical methods are: Finite-Differences, Finite-Elements, Finite-Volume and Analytic-Element, though the first two are the most popular. We shall discuss the methods of finite differences and finite elements, which are the most popular techniques and the method of finite volume which is more recent but becoming increasingly more popular in fluid dynamics and which is also the technique that will be employed in this work.

4.2.1 Finite Difference Method

The finite difference method (FDM) is the most widely used numerical method in groundwater studies. Majority of the publicly available computer codes for groundwater flow and contaminant transport modelling are based on the FDM. For example, MODFLOW, a FORTRAN program developed by the U.S. Geological Survey for three-dimensional flow modelling (Fitts, 2002). Some of the reasons for the FDM popularity is its versatility, simplicity and also the fact that its theoretical foundations are firm.

The first step in the implementation of the FDM is to draw an orthogonal grid across the modelled domain. This is obtained by dividing the axes into segments and drawing lines parallel to the axes. The segments on the axes may be equal (uniform grid) or different (nonuniform grid). In general, lines are made closer in areas where we wish to obtain more detailed information on the behaviour of the state variable. The blocks formed by these lines are called cells. By replacing the derivatives that appear in the partial differential equations by finite difference expressions written in terms of the values of the dependent variable at the grid points (nodes), we obtain the finite difference equations of the problem. One FDM scheme places nodes at the center of each cell (block-centered grid) and another places them at the intersections of the grid lines (mesh-centered grid) as shown in Figures 4.1 and 4.2. The choice of the type of grid to use depends largely on the boundary conditions. The mesh-centered grid is convenient for problems where values of head are specified on the boundary, whereas the block-centered grid has an advantage where the flux is specified across the boundary (Faust & Mercer, 1980).

The solution of the difference equation, or the set of difference equations, is carried out numerically, usually by means of a computer. If we denote the exact solution of the partial differential equation by h_{exac}, the exact solution of the difference equations by h_{FD} and the numerical solution of the difference equations by h_{num}, we call $|h_{\text{exac}} - h_{\text{FD}}|$ the truncation

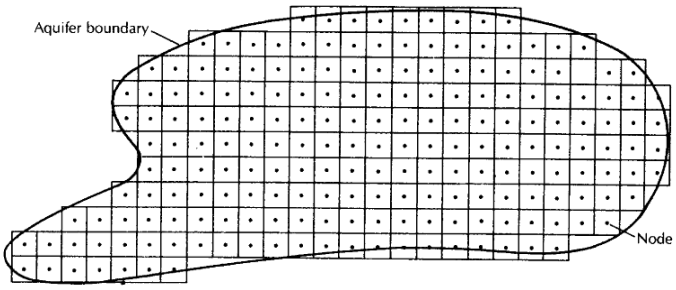

Figure 4.1: Block-centered finite-difference grid.

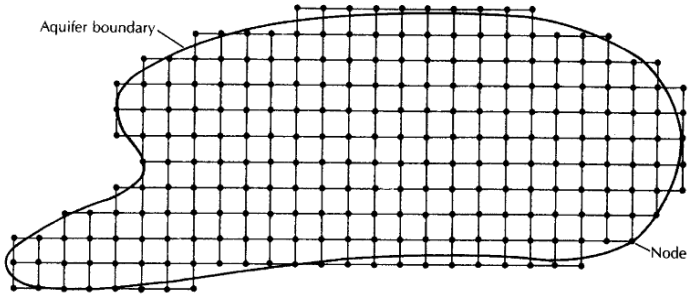

Figure 4.2: Mesh-centered finite-difference grid

error, due to the truncation of the Taylor series expansion in the finite difference formulation, and $|h_{\text{FD}} - h_{\text{num}}|$ the numerical roundoff error, due to the inability of the computer to carry numbers to an infinite number of digits. The condition for convergence of the solution is that $|h_{\text{exac}} - h_{\text{FD}}| \to 0$ everywhere in the solution domain as the grid size $\Delta x, \Delta y$, etc is made smaller,that is, approaching zero. The condition for stability is that given an error in the solution process, either from truncation, or from roundoff, that error will not grow exponentially from one time step to the next (Bear & Cheng, 2010). The objective is to find h_{num} such that over the whole region of interest $|h_{\text{exac}} - h_{\text{num}}|$ is smaller than some error criterion.

Let us demonstrate the FDM approach that uses the block-centered grid by applying it on our problem model equation (3.5):

$$\frac{\partial^2 h}{\partial x^2} + \frac{\partial^2 h}{\partial y^2} = \frac{S}{T}\frac{\partial h}{\partial t} \tag{4.3}$$

$$h(300, y, t) = h(x, 300, t) = 12$$
$$\frac{\partial h}{\partial x}(0, y, t) = \frac{\partial h}{\partial y}(x, 0, t) = 0$$
$$h(x, y, 0) = 10$$

The derivatives that appear in equation (4.3) may be approximated by either using truncated Taylor series, or by carrying out a mass balance over a finite difference block. We present the latter approach based on Freeze and Cherry (1979).

Consider an interior block and the four blocks connected to it, Figure 4.3 (b). The center block is labelled 5 and Q_{15}, for example, represents the volumetric flux from block 1 to block 5; Δx and Δy are the nodal spacings in the $x-$ and $y-$direction, respectively. The continuity

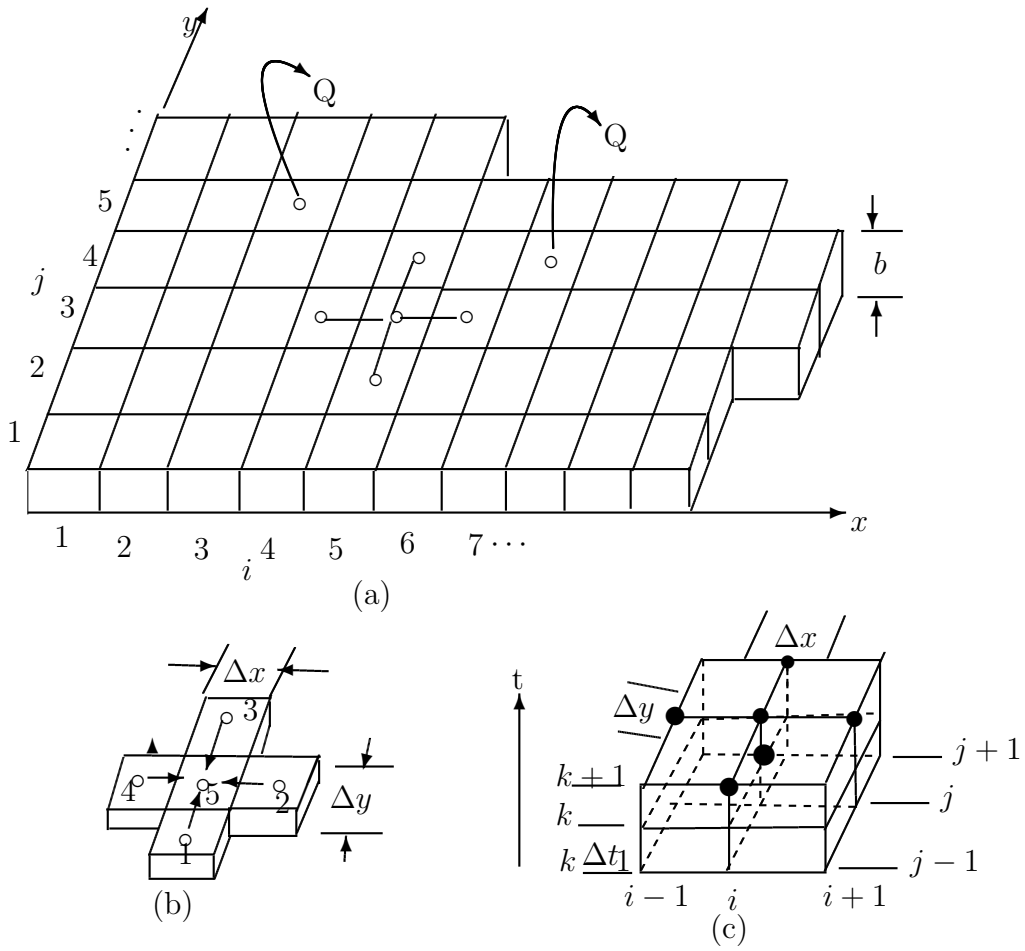

Figure 4.3: Finite-difference discretization of a two-dimensional, horizontal, confined aquifer

principle states that the net rate of flow into any block must be equal to the time rate of

change of storage within that block. Thus a mass balance for block 5 may be written as

$$Q_{15} + Q_{25} + Q_{35} + Q_{45} = S_s \Delta x \Delta y b \frac{\partial h_5}{\partial t} \tag{4.4}$$

From Darcy's law, flux Q_{15} can be evaluated as

$$Q_{15} = K \frac{h_1 - h_5}{\Delta y} \Delta x b \tag{4.5}$$

Similar expressions can be written for Q_{25}, Q_{35} and Q_{45} and substitution into equation (4.4) gives

$$Kb \left(\frac{h_1 - h_5}{\Delta y} \Delta x + \frac{h_2 - h_5}{\Delta x} \Delta y + \frac{h_3 - h_5}{\Delta y} \Delta x + \frac{h_4 - h_5}{\Delta x} \Delta y \right) = S_s b \Delta x \Delta y \frac{\partial h_5}{\partial t} \tag{4.6}$$

Now, using the fact that $T = Kb$ and $S = S_s b$ and dividing through by $\Delta x \Delta y$, Equation (4.6) may be written as

$$\left(\frac{h_2 - 2h_5 + h_4}{(\Delta x)^2} + \frac{h_1 - 2h_5 + h_3}{(\Delta y)^2} \right) = \frac{S}{T} \frac{\partial h_5}{\partial t} \tag{4.7}$$

The time derivative on the right-hand side of equation (4.7) may be approximated by a backward difference:

$$\frac{\partial h_5}{\partial t} = \frac{h_5(t) - h_5(t - \Delta t)}{\Delta t}, \tag{4.8}$$

where Δt is the time step. Converting to the ijk notation indicated on Figure 4.3 (c), we have

$$\frac{h_{i+1,j}^{k+1} - 2h_{i,j}^{k+1} + h_{i-1,j}^{k+1}}{(\Delta x)^2} + \frac{h_{i,j-1}^{k+1} - 2h_{i,j}^{k+1} + h_{i,j+1}^{k+1}}{(\Delta y)^2} = \frac{S}{T \Delta t} (h_{i,j}^{k+1} - h_{i,j}^{k}) \tag{4.9}$$

which is the finite-difference equation for an internal node (i, j), $2 \leq i, j \leq N-1$. The nodes in the boundary blocks ($i, j = 1$ and $i, j = N$) require special consideration by taking into account the boundary conditions. We shall demonstrate the treatment of boundary nodes in Section 4.2.3.

The values of the parameters $\Delta x, \Delta y, \Delta t, S$ and T are known as is the value of the hydraulic head, $h_{i,j}^k$. Writing an equation similar to (4.9) for each node results in $n = N^2$ linear, algebraic equations in n unknowns. This set of equations must be solved simultaneously at each time step, starting from a set of initial conditions where $h_{i,j}$ is known for all (i, j) and

proceeding through the time steps, $k = 1, 2, 3, \ldots$.

4.2.2 Finite Element Method

The finite element method (FEM) is another widely used numerical technique employed in groundwater modelling. The term FEM was introduced by Clough (1960) while working on problems in structural mechanics but the method dates back to Courant (1943) who used the works of Ritz (1908) and Galerkin (1915) to approximate solutions to elliptic PDEs (Bear & Cheng, 2010; Schäfer, 2006). The main attributes of the FEM is its ability to model problems defined on complex geometries, the consistent treatment of differential-type boundary conditions and the possibility to be programmed in a flexible and general purpose format (Donea & Huerta, 2003). The flexibility of the FEM is useful in solving coupled problems, such as contaminant transport, or in solving moving boundary problems, such as a moving water table (Wang & Anderson, 1982).

Standard FEM applications in groundwater are based on the Galerkin formulation of the method of weighted residuals. In the weighted residual method, a solution to the governing PDE is approximated by a piecewise function $\hat{h}$. The governing PDE is precisely satisfied by the exact solution h. If the piecewise approximating function $\hat{h}$ is substituted into the equation, it will not hold exactly and a residual is defined to measure the errors. The method seeks to minimise the residuals in some sense by multiplying them by a set of weighting functions and integrating. As a result we obtain a set of algebraic equations for the unknown coefficients of the approximating functions. We briefly describe the weighted residual method.

Weighted residual methods are numerical procedures for approximating the solution of a set of differential (or integral) equations of the form

$$\mathcal{L}(h(\mathbf{x})) = f(\mathbf{x}), \quad \mathbf{x} \in \Omega \subset \mathbb{R}^2 \tag{4.10}$$

with boundary conditions

$$\mathcal{B}(h(\mathbf{x})) = g(\mathbf{x}), \quad \mathbf{x} \in \partial\Omega \tag{4.11}$$

where $\mathbf{x}$ represents the spatial coordinates (x, y) and Ω is the solution domain bounded by $\partial\Omega$. The boundary $\partial\Omega$ is usually divided into two parts that cover the whole of $\partial\Omega$ and do not overlap:

- the essential (Dirichlet) boundary $\partial\Omega_D$ and
- the natural (Neumann) boundary $\partial\Omega_N$

A Dirichlet boundary condition prescribes the value of the dependent variable at the boundary, e.g. $h(x) =$ constant while the Neumann boundary condition prescribes the gradient normal to the boundary of a variable at the boundary, e.g. $\partial_n h(x) =$ constant.

One basic approach to finding an approximate solution $\hat{h}$ is to express it as (Bear & Cheng, 2010; Connor & Brebbia, 1976):

$$h(\mathbf{x}) \approx \hat{h}(\mathbf{x}) = \sum_{k=1}^{n} \alpha_k \phi_k(\mathbf{x}), \;\; \mathbf{x} \in \Omega \tag{4.12}$$

where ϕ_k are linearly independent functions, known as basis functions, taken from a complete sequence(Connor & Brebbia, 1976) and α_k are unknown coefficients to be determined. One requirement is that the basis functions should satisfy the boundary conditions of the problem and have the necessary degree of continuity so as to make the left-hand side of (4.10) different from zero (Connor & Brebbia, 1976).

Substitution of (4.12) into (4.10) produces an error, R, called the residual:

$$R(\mathbf{x}) = \mathcal{L}(\hat{h}(\mathbf{x})) - \mathcal{L}(h(\mathbf{x})) = \mathcal{L}(\hat{h}(\mathbf{x})) - f(\mathbf{x}) \neq 0 \tag{4.13}$$

Note that the residual is zero for the exact solution. The method of weighted residuals determines the unknown coefficients by minimizing the error. This is accomplished by setting integrals of the weighted residual equal to zero over the entire domain:

$$\int_{\Omega} R(\mathbf{x})\omega_i(\mathbf{x})d\mathbf{x} = \int_{\Omega} \Big[\mathcal{L}(\hat{h}(\mathbf{x})) - f(\mathbf{x})\Big]\, \omega_i(\mathbf{x})d\mathbf{x} = 0 \tag{4.14}$$

for a finite set of weighting functions $\omega_i(\mathbf{x})$, $i = 1, 2, \ldots, n$. Different choices of the weighting function lead to different numerical methods.

In the Galerkin method, the weighting functions are chosen to be identical to the basis functions. In other words, equation (4.14) becomes

$$\int_{\Omega} \Big[\mathcal{L}(\hat{h}(\mathbf{x})) - f(\mathbf{x})\Big]\, \omega_i(\mathbf{x})d\mathbf{x} = \int_{\Omega} \left[\mathcal{L}(\sum_{k=1}^{n} \alpha_k \phi_k(\mathbf{x})) - f(\mathbf{x})\right] \phi_i(\mathbf{x})d\mathbf{x} = 0 \tag{4.15}$$

The integral in equation (4.15) is simplified using integration by parts and since the basis

and weighting functions are defined to be of a specific algebraic form (e.g. linear basis functions), this integral is straightforward to solve and becomes a set of n simultaneous algebraic equations.

In the FEM, the solution domain is subdivided into a large number of elements and rather than defining a single continuous, global function for the approximate solution, we represent the solution by using a number of local interpolation functions, each defined within a given element. We then patch them together to form a piecewise continuous function (Bear & Cheng, 2010). Within each element, the solution is represented by a small number of discrete values, and a low degree polynomial is used for the interpolation. The general methodology of the FEM involves the following steps:

(i) Divide the domain into a number of finite-sized subdomains called elements. Each element is represented by a finite number of grid points (nodes). The most common shapes for the finite elements are triangles for two-dimensional flow and triangular prisms for three-dimensional flow. The triangles intersect at nodes that represent the points at which the unknown quantities, such as heads, will be computed (see Figure 4.4).

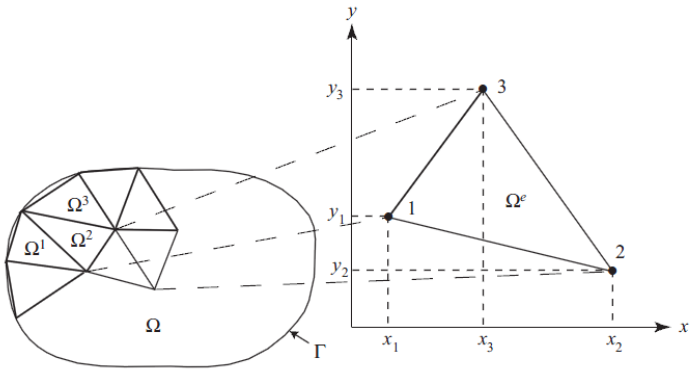

Figure 4.4: Dividing the domain into triangular elements (Bear & Cheng, 2010)

(ii) Assume a profile function $\hat{h}$ to represent the head variation within each element. The functions are defined within the element using the nodal values of the element. Linear, quadratic and cubic polynomials are frequently used functions because they are easy to work with (Logan, 2007). Inside the element, $\hat{h}$ is a linear function satisfying the condition that $\hat{h} = h_1, h_2$ and h_3 at the three nodes $1, 2, 3$ and can be expressed as:

$$\hat{h} = \sum_{i=1}^{3} h_i \phi_i \tag{4.16}$$

where h_i is the head value at node i and ϕ_i are linear basis functions ($\phi_i = a_i + b_i x + c_i y$) defined by $\phi_i = 1$ at node i and zero at the other two nodes (Bear & Cheng, 2010; Fitts, 2002). By patching the Ω^e elements together, the approximate function becomees

$$\hat{h} = \sum_{e=1}^{n_e} \sum_{i=1}^{3} h_i \phi_i \tag{4.17}$$

and after sorting the terms for the nodal values h_j, $j = 1, \ldots, m$, where j is the node's global index, m is the total number of nodes in the FEM grid, equation (4.17) can be expressed as

$$\hat{h} = \sum_{j=1}^{m} h_j \phi_j = \Phi \mathbf{h} \tag{4.18}$$

where ϕ_j is the combined shape function, incorporating all the contributions to the $j - th$ node.

(iii) Derive the equations and stiffness matrix using the Galerkin formulation of the method of weighted residuals and incorporate boundary conditions.

(iv) Solve the system of global equations for the head values at the nodal points.

Consider the model problem (3.5) as given by equation (4.19):

$$\frac{\partial^2 h}{\partial x^2} + \frac{\partial^2 h}{\partial y^2} = \frac{S}{T} \frac{\partial h}{\partial t} \tag{4.19}$$

with the boundary conditions

$$\begin{aligned} h(300, y, t) = h(x, 300, t) &= 12 \\ -\frac{\partial h}{\partial \mathbf{n}} &= 0, x = 0, y = 0 \\ h(x, y, 0) &= 10 \end{aligned} \tag{4.20}$$

The approach to solving this problem with the FEM is based upon writing it in a different form, which is sometimes called the weak or variational form. Based on the Galerkin weighted residual method, we use the shape functions ϕ_i as the weighting functions and minimize the

residuals of the governing equation and the boundary conditions:

$$\int_0^{300}\int_0^{300}\left(\nabla^2 h - \frac{S}{T}\frac{\partial h}{\partial t}\right)\phi_i\, dxdy + \int_{300}^{0}\phi_i\frac{\partial h}{\partial x}(t,0,y)dy + \int_0^{300}\phi_i\frac{\partial h}{\partial y}(t,x,0)dx = 0. \tag{4.21}$$

The residual of the Dirichlet boundary condition is not included because it is automatically satisfied by the adoption of the approximation function (4.18) that uses the nodal head values for interpolation (Bear & Cheng, 2010). Equation (4.21) is called a *strong formulation* of the problem, because, when it is satisfied for an arbitrary weighting function at all points of Ω, the original PDE (4.19) must be satisfied at all points (Bear & Cheng, 2010).

It should be noted that in order to satisfy the PDE equation, the function h must be at least twice differentiable. This poses a problem for the piecewise linear approximation (4.17) which becomes zero when differentiated twice hence making equation (4.21) vanish. Although this problem can be solved by using higher degree polynomials, this is not done in FEM since it makes the element more complicated. Hence rather than increase the degree of the polynomial approximation, we reduce the formulation's differentiation requirement by introducing the *weak formulation* (Bear & Cheng, 2010). This is accomplished by making use of Green's theorem, which is the multidimensional extension of integration by parts.

Theorem 4.2.1. *(Green's Theorem (Kellogg, 1929)) Let Ω denote a closed regular region of space and let U and V be two functions defined on Ω and continuous in Ω together with their partial derivatives of the first order. Moreover, let U have continuous derivatives of the second order in Ω. Then*

$$\int_\Omega V\nabla^2 U\, d\boldsymbol{x} + \int_\Omega (\nabla U\cdot\nabla V)\, d\boldsymbol{x} = \int_{\partial\Omega} V\frac{\partial U}{\partial \mathbf{n}}\, d\boldsymbol{x} \tag{4.22}$$

where $\mathbf{n}$ means the outwardly directed normal to the surface $\partial\Omega$ bounding Ω

Thus by applying Green's theorem,

$$\begin{aligned}\int_0^{300}\int_0^{300}\phi_i\nabla^2 h\, dxdy = &-\int_0^{300}\int_0^{300}\nabla\phi_i\cdot\nabla h\, dxdy - \int_0^{300}\phi_i\frac{\partial h}{\partial y}(t,x,0)\, dx \\ &+\int_0^{300}\phi_i\frac{\partial h}{\partial x}(t,300,y)\, dy + \int_{300}^{0}\phi_i\frac{\partial h}{\partial y}(t,x,300)\, dx - \int_{300}^{0}\phi_i\frac{\partial h}{\partial x}(t,0,y)\, dy\end{aligned} \tag{4.23}$$

and substituting (4.23) into (4.21) and simplifying, we obtain

$$\int_0^{300}\int_0^{300} \nabla\phi_i \cdot \nabla h \, dxdy + \int_0^{300}\int_0^{300} \frac{S}{T}\phi_i \frac{\partial h}{\partial t} \, dxdy - \int_{300}^{0} \phi_i \frac{\partial h}{\partial y}(t, x, 300) \, dx - \int_0^{300} \phi_i \frac{\partial h}{\partial x}(t, 300, y) \, dy = 0 \tag{4.24}$$

Since the shape functions ϕ_i, also selected as the weighting functions, vanish at the Dirichlet boundary, equation (4.24) becomes

$$\int_0^{300}\int_0^{300} \nabla\phi_i \cdot \nabla h \, dxdy + \int_0^{300}\int_0^{300} \frac{S}{T}\phi_i \frac{\partial h}{\partial t} \, dxdy = 0 \tag{4.25}$$

and this is the weak formulation of problem (4.19) and (4.20). It should be noted that in the weak formulation, h is differentiated only once and can thus be represented by the linear shape function Φ. Another reason for using the weak formulation is that when the shape function Φ is used to approximate h, the solution matrix representing the linear system is symmetric, which means a significant reduction in computational effort (Bear & Cheng, 2010).

We now substitute the piecewise approximation (4.18) into (4.25), which gives

$$\left[\int_0^{300}\int_0^{300} \nabla\phi_i \cdot \nabla\Phi \, dxdy\right] \mathbf{h} + \left[\int_0^{300}\int_0^{300} \frac{S}{T}\phi_i\Phi \, dxdy\right] \frac{\partial \mathbf{h}}{\partial t} = 0 \tag{4.26}$$

where $\mathbf{h}$ denotes the column vector of the discrete nodal values of h. Note also that the discrete head values, $\mathbf{h}$, are not functions of space and can thus be moved out of the integration. Executing equation (4.26) for the n nodes, $i = 1, 2, \ldots, n$, we obtain the matrix equation

$$A\mathbf{h} + B\frac{\partial \mathbf{h}}{\partial t} = 0 \tag{4.27}$$

where A and B are $N \times N$ matrices with components

$$A_{ij} = \int_0^{300}\int_0^{300} \nabla\phi_i \cdot \nabla\phi_j \, dxdy, \quad \text{and} \tag{4.28}$$

$$B_{ij} = \int_0^{300}\int_0^{300} \frac{S}{T}\phi_i\phi_j \, dxdy \tag{4.29}$$

The time derivative can be approximated using a first order forward difference

$$\frac{\partial \mathbf{h}}{\partial t} = \frac{\mathbf{h}^{k+1} - \mathbf{h}^k}{\Delta t} \tag{4.30}$$

and the rest of the $\mathbf{h}$ terms in equation (4.27) can be represented as a weighted average between the two time levels k and $k+1$;

$$\mathbf{h} = (1-\theta)\mathbf{h}^k + \theta\mathbf{h}^{k+1} \tag{4.31}$$

where $0 \leq \theta \leq 1$ is a weighting factor for the time discretization. Hence equation (4.27) can be expressed as

$$(1-\theta)A\mathbf{h}^k + \theta A\mathbf{h}^{k+1} + \frac{1}{\Delta t}B(\mathbf{h}^{k+1} - \mathbf{h}^k) = 0 \tag{4.32}$$

where we know $\mathbf{h}$ at time level k and seek the solution at time level $k+1$. Setting $\theta = 0$ gives the explicit scheme, which is conditionally stable. $\theta = 1$ gives the implicit scheme and $\theta = \frac{1}{2}$ the Crank-Nicholson scheme, which are both unconditionally stable (Bear & Cheng, 2010).

4.2.3 Finite Volume Method

One disadvantage of the FDM is that, since it relies on a regular grid to approximate a considered domain, it has a rigidity in conforming to complex boundary geometries which results in loss of accuracy in predicting hydraulic heads along and near the boundaries(Bear & Cheng, 2010; Loudyi et al., 2007). Barrash and Dougherty (1997) also found that the FDM underestimated large head gradients that can occur in the vicinity of pumping or injection wells. Another drawback is that, since the partial differential equations for groundwater are derived using the principle of mass conservation, we would expect the discretized equations to physically reflect the same conservation. Since the FDM equations can be derived mathematically using expanded Taylor series, conservativeness is not generally an inbuilt part of the FDM discretization. Some of these limitations can be addressed by using techniques of mesh refinement. However, fine grids can result in long execution times that prohibit the many model runs often needed to understand the system dynamics and calibrate the model (Loudyi et al., 2007).

An alternative to grid refinement is to use techniques in which the grid can be made more flexible. Among the latest techniques to be developed is the finite volume method (FVM), which is based on the integration of the governing equations of fluid flow over a control volume that can have any shape with rectilinear sides, structured or unstructured and with flow variables associated with a point inside the cell (cell-centered FVM) or attached to cell vertices (cell-vertex FVM)(Loudyi et al., 2007). Compared to the FDM, the FVM has the

following advantages:

(i) Spatial discretization is totally flexible: the FVM allows the distortion of a rectilinear mesh to conform to the geometry of a problem's boundary, in the sense that the line joining two grid points does not necessarily have to be perpendicular to a given control volume surface and the mesh can be refined locally to give more resolution in regions of particular interest.

(ii) The FVM is based on the integral form of the conservation principle. Unlike the node-centered FDM, where the conservation principle is satisfied only if the grid size approaches zero, the FVM conserves the extensive quantity within each control volume. The block-centered FDM has a similar property and can be considered as a special case of the FVM, using a cell-centered, cartesian, uniform grid (Bear & Cheng, 2010).

(iii) Because of (ii), there is no need for dependent variables to be differentiable everywhere which means that a larger class of problems can be solved.

The basic methodology of the FVM involves three steps:

(i) Divide the domain into a number of finite-sized subdomains called control volumes. Each control volume is represented by a finite number of grid points. The control volumes in a two-dimensional structured mesh are usually convex quadrilaterals. The structured mesh makes it possible to keep track of the cells and grid nodes by their row and column numbers. It is however limited in its ability to conform to a complex geometry of a problem boundary. A more conforming unstructured mesh can be developed for the FVM by using triagular shaped cells. The location of adjoining cells are not known automatically and must be stored which results in more complicated data structures. It could be argued that, for complex geometries, unstructured meshes are easier to generate than structured ones (Causon, Mingham, & Qian, 2011).

(ii) Integrate the governing differential equation over each control volume and apply the divergence theorem. Once we do that, we eventually get integral expressions.

(iii) Consider a profile assumption for the dependent variable to approximate the derivative terms. The result is a set of linear algebraic equations, one for each control volume. These equations can then be solved iteratively or simultaneously.

Theorem 4.2.2. *(Divergence Theorem) Let V be a simply connected region in the xy-plane enclosed by a piecewise smooth curve ∂V. Let n be the unit outward-pointing normal to ∂V.*

Then

$$\int_V \nabla \cdot F dV = \int_{\partial V} F \cdot n dX$$

where dV is the element of area and dX is the element of length.

Consider our two-dimensional model equation (3.5);

$$\nabla \cdot \nabla h = \frac{S}{T}\frac{\partial h}{\partial t} \tag{4.33}$$

with the boundary conditions

$$\begin{aligned} h(t, 300, y) = h(t, x, 300) &= 12 \\ -\frac{\partial h}{\partial \mathbf{n}} &= 0, x = 0, y = 0 \\ h(0, x, y) &= 10 \end{aligned} \tag{4.34}$$

We can average the equation (4.33) by integrating it over an arbitrary control volume V:

$$\int_V \nabla \cdot (\nabla h) dV = \int_V \frac{S}{T}\frac{\partial h}{\partial t} dV \tag{4.35}$$

and applying the divergence (Gauss) theorem yields:

$$\int_S \nabla h \cdot \mathbf{n} dS = \int_V \frac{S}{T}\frac{\partial h}{\partial t} dV \tag{4.36}$$

where S is the surface of the control volume and $\mathbf{n}$ represents the outward unit normal to the surface.

Using quadrilateral control volumes on a uniform cartesian mesh (see Figure 4.5), the surface integral in (4.36) can be split into the sum of the four surface integrals over the cell faces S_c ($c = e, w, n, s$) of the control volume, such that the balance equation (4.36)can be equivalently written in the form

$$\sum_c \int_{S_c} \nabla h \cdot \mathbf{n}_c dS_c = \int_V \frac{S}{T}\frac{\partial h}{\partial t} dV \tag{4.37}$$

The integrals appearing in (4.37) can be approximated by the average values at the midpoints

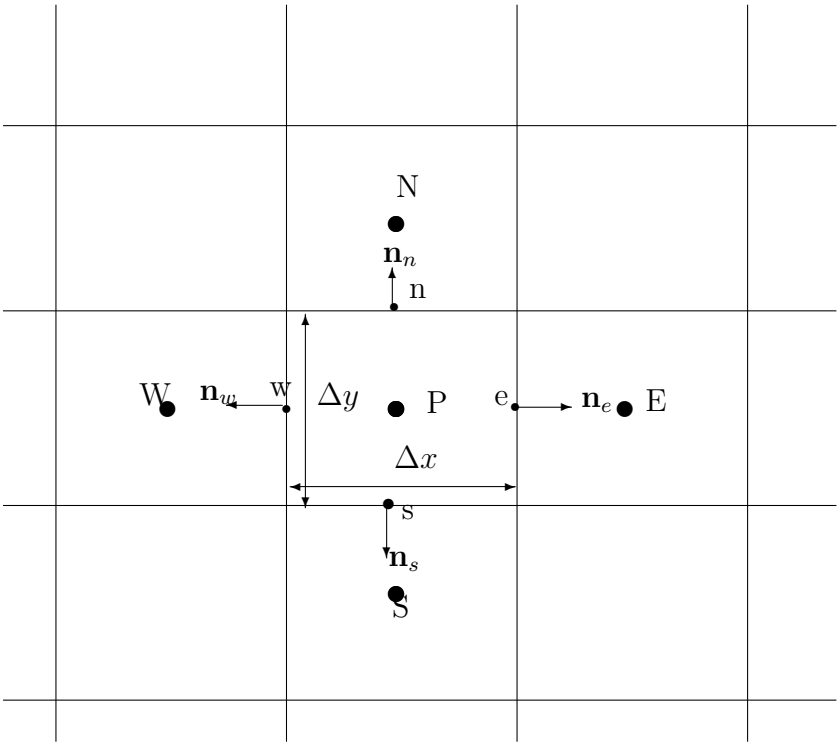

Figure 4.5: Schematic view of a finite-volume quadrilateral cell system

of the faces and at the centre of the control volume (Schäfer, 2006):

$$\int_{S_c} \nabla h \cdot \mathbf{n}_c dS_c \approx S_c((\nabla h)_c^m \cdot \mathbf{n}_c) \text{ and } \int_V \frac{S}{T}\frac{\partial h}{\partial t} dV \approx \frac{S}{T}\left(\frac{\partial h}{\partial t}\right)_P V \tag{4.38}$$

and substituting in (4.37) yields:

$$\sum_c S_c((\nabla h)_c^m \cdot \mathbf{n}_c) = \frac{S}{T}\left(\frac{\partial h}{\partial t}\right)_P V \tag{4.39}$$

where S_c is the length of the control volume face, $(\nabla h)_c^m$ is the hydraulic gradient at the midpoint of the control volume face, $\left(\frac{\partial h}{\partial t}\right)_P$ is the time derivative at the center of the control volume and V is the volume (area in 2D) of the control volume.

Now using a first order forward difference in time and using the fact that $S_e = S_w = \Delta y$, $S_n = S_s = \Delta x$ and $V = \Delta x \Delta y$, equation (4.39) can be written as

$$\Delta x((\nabla h)_n^m \cdot \mathbf{n}_n + (\nabla h)_s^m \cdot \mathbf{n}_s) + \Delta y((\nabla h)_e^m \cdot \mathbf{n}_e + (\nabla h)_w^m \cdot \mathbf{n}_w) = \frac{S}{T}\frac{h_P^{k+1} - h_P^k}{\Delta t}\Delta x \Delta y. \tag{4.40}$$

Note, for example, that

$$(\nabla h)_n^m \cdot \mathbf{n}_n = \left(\frac{\partial h}{\partial x}, \frac{\partial h}{\partial y}\right)_n^m \cdot (0,1) = \left(\frac{\partial h}{\partial y}\right)_n^m. \tag{4.41}$$

Thus equation (4.40) can be simplified to

$$\Delta x \left(\left(\frac{\partial h}{\partial y}\right)_n^m - \left(\frac{\partial h}{\partial y}\right)_s^m\right) + \Delta y \left(\left(\frac{\partial h}{\partial x}\right)_e^m - \left(\frac{\partial h}{\partial x}\right)_w^m\right) = \frac{S}{T}\frac{h_P^{k+1} - h_P^k}{\Delta t}\Delta x \Delta y. \tag{4.42}$$

The main challenge of the FVM is the approximation of the gradients (or fluxes) at the cell faces. The accuracy of a control volume discretization depends heavily on the approximation of the flux at the midpoint of the control volume faces and many methods have been proposed to approximate the gradient along a control volume surface for different computational fluid dynamics applications (Loudyi et al., 2007; Jayantha & W.Turner, 2001, 2003). To calculate the gradients at the midpoint of the cell faces, an approximate distribution of properties between nodal points is used (Versteeg & Malalasekera, 1995). The simplest and most obvious technique is the central differencing scheme (CDS) which which assumes that h is a linear function between any two node points and a second order approximation for the gradients is given (Schäfer, 2006):

$$\left(\frac{\partial h}{\partial x}\right)_e^m \approx \frac{h_E - h_P}{x_E - x_P} = \frac{h_E - h_P}{\Delta x} \quad \text{and} \quad \left(\frac{\partial h}{\partial y}\right)_n^m \approx \frac{h_N - h_P}{\Delta y} \tag{4.43}$$

The time level at which these derivatives are computed determines whether the scheme is explicit (k), implicit ($k+1$) or Crank-Nicholson (mixture of both previous and new time levels). Using an implicit scheme and substituting (4.43) into (4.42), we get the following equation:

$$\Delta x \left(\frac{h_N^{k+1} - h_P^{k+1}}{\Delta y} - \frac{h_P^{k+1} - h_S^{k+1}}{\Delta y}\right) + \Delta y \left(\frac{h_E^{k+1} - h_P^{k+1}}{\Delta x} - \frac{h_P^{k+1} - h_W^{k+1}}{\Delta x}\right) = \frac{S}{T}\frac{h_P^{k+1} - h_P^k}{\Delta t}\Delta x \Delta y \tag{4.44}$$

which can be simplified to

$$\frac{h_N^{k+1} - 2h_P^{k+1} + h_S^{k+1}}{(\Delta y)^2} + \frac{h_E^{k+1} - 2h_P^{k+1} + h_W^{k+1}}{(\Delta x)^2} = \frac{S}{T\Delta t}(h_P^{k+1} - h_P^k) \tag{4.45}$$

Using the (i, j) notation, we have

$$\frac{h_{i,j+1}^{k+1} - 2h_{i,j}^{k+1} + h_{i,j-1}^{k+1}}{(\Delta y)^2} + \frac{h_{i+1,j}^{k+1} - 2h_{i,j}^{k+1} + h_{i-1,j}^{k+1}}{(\Delta x)^2} = \frac{S}{T\Delta t}(h_{i,j}^{k+1} - h_{i,j}^{k}) \tag{4.46}$$

which is the FVM equation at the interior node P or $2 \leq i, j \leq N-1$. Note that this equation is common to both the cell-centered FDM and the FVM.

To complete the scheme (4.46) we need to update the formula also for the boundary cell nodes $i = 1, j = 1, i = N$ and $j = N$. These must be derived by taking the boundary conditions (4.34) into account. We introduce the ghost cells $i = 0, j = 0, i = N+1$ and $j = N+1$ which are located just outside the domain (Figure 4.6). The boundary conditions are used to fill these cells with values $h_{0,j}, h_{i,0}, h_{N+1,j}$ and $h_{i,N+1}$, based on the values $h_{i,j}$ in the interior cells. The same formula (4.46) can then be used also for $i, j = 1$ and $i, j = N$.

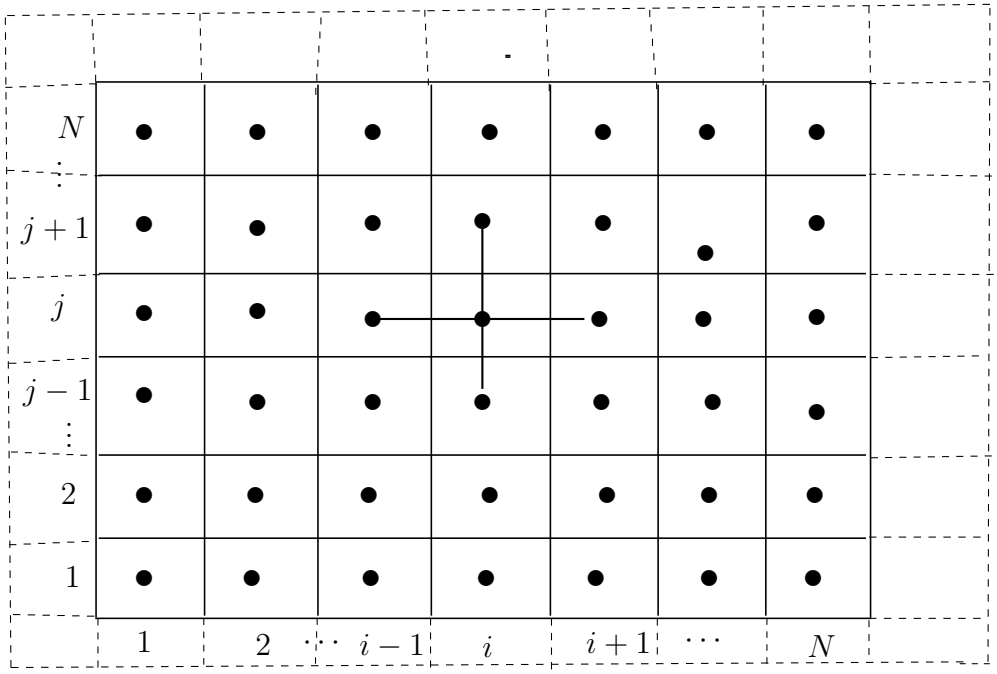

Figure 4.6: Discretized domain with ghost cells in dotted lines

Consider the Neumann boundary condition $\dfrac{\partial h}{\partial \mathbf{n}} = 0$ at $x = 0$ and $y = 0$. We formally extend the definition of the solution h for $(x, y) < 0$, that is, outside the domain.
At $x = 0$,

$$\frac{\partial h}{\partial \mathbf{n}} = 0 = \nabla h \cdot (-1, 0) = \left(\frac{\partial h}{\partial x}, \frac{\partial h}{\partial y}\right) \cdot (-1, 0) = -\frac{\partial h}{\partial x}, \tag{4.47}$$

or $h_x(t,0,y)=0$. Now

$$\begin{aligned} 0 =& h_x(t,0,y) = \frac{h(t,x_1,y)-h(t,x_0,y)}{\Delta x} + O((\Delta x)^2) \\ =& \frac{h_{1,j}-h_{0,j}}{\Delta x} + O((\Delta x)^2) \;\Rightarrow\; h_{0,j} = h_{1,j} + O((\Delta x)^3). \end{aligned} \tag{4.48}$$

Dropping the $O((\Delta x)^3)$ term, we get get an expression for $h_{0,j}$ in terms of $h_{1,j}$:

$$h_{0,j} = h_{1,j}. \tag{4.49}$$

Similarly $h_y(t,x,0)=0 \;\Rightarrow\; h_{i,0}=h_{i,1}$.

The Dirichlet boundary conditions $h(t,300,y)=h(t,x,300)=0.5$ can be approximated to second order by taking the average of two cells to approximate the value in between,

$$12 = h(t,x,300) = \frac{h(t,x,y_N)+h(t,x,y_{N+1})}{2} + O((\Delta y)^2) = \frac{h_{i,N}+h_{i,N+1}}{2} + O((\Delta y)^2) \tag{4.50}$$

leading to the approximation

$$h_{i,N+1} = 24 - h_{i,N}. \tag{4.51}$$

Similarly, $h_{N+1,j}=24-h_{N,j}$. In the approximation of h in the ghost cells, we use a second order approximation so that we do not compromise the already second order discretization of the equation.

If we let $\Delta y=\Delta x$, then equation (4.46) becomes

$$h^{k+1}_{i,j+1} + h^{k+1}_{i,j-1} + h^{k+1}_{i+1,j} + h^{k+1}_{i-1,j} - 4h^{k+1}_{i,j} = \frac{(\Delta x)^2 S}{T\Delta t}(h^{k+1}_{i,j} - h^{k}_{i,j}). \tag{4.52}$$

Rearranging terms with $k+1$ on the left and terms with k on the right hand side gives

$$h^{k+1}_{i,j+1} + h^{k+1}_{i,j-1} + h^{k+1}_{i+1,j} + h^{k+1}_{i-1,j} - \left(4 + \frac{(\Delta x)^2 S}{T\Delta t}\right) h^{k+1}_{i,j} = -\frac{(\Delta x)^2 S}{T\Delta t} h^{k}_{i,j}. \tag{4.53}$$

Letting $M = \dfrac{(\Delta x)^2 S}{T\Delta t}$, equation (4.53) can be written as

$$h^{k+1}_{i,j+1} + h^{k+1}_{i,j-1} + h^{k+1}_{i+1,j} + h^{k+1}_{i-1,j} - (4+M)\, h^{k+1}_{i,j} = -M h^{k}_{i,j}. \tag{4.54}$$

The cross in the middle of Figure 4.6 is called the 5-point stencil of equation (4.54), because it connects all the five values of h present in equation (4.54). Equation (4.54) together with the boundary conditions defines a set of $n = N^2$ linear equations in the n unknowns $h_{i,j}$ for $1 \leq i, j \leq N$.

The n equations represented by equation (4.54) can be expressed as a single matrix equation $\mathbf{Ah}^{k+1} = \mathbf{b}$ by writing the unknowns $h_{i,j}$ in a single long n-by-1 vector. This requires us to choose an order for them and we arbitrarily choose to number them as shown in Figure 4.7 row wise from the lower left to the upper right.

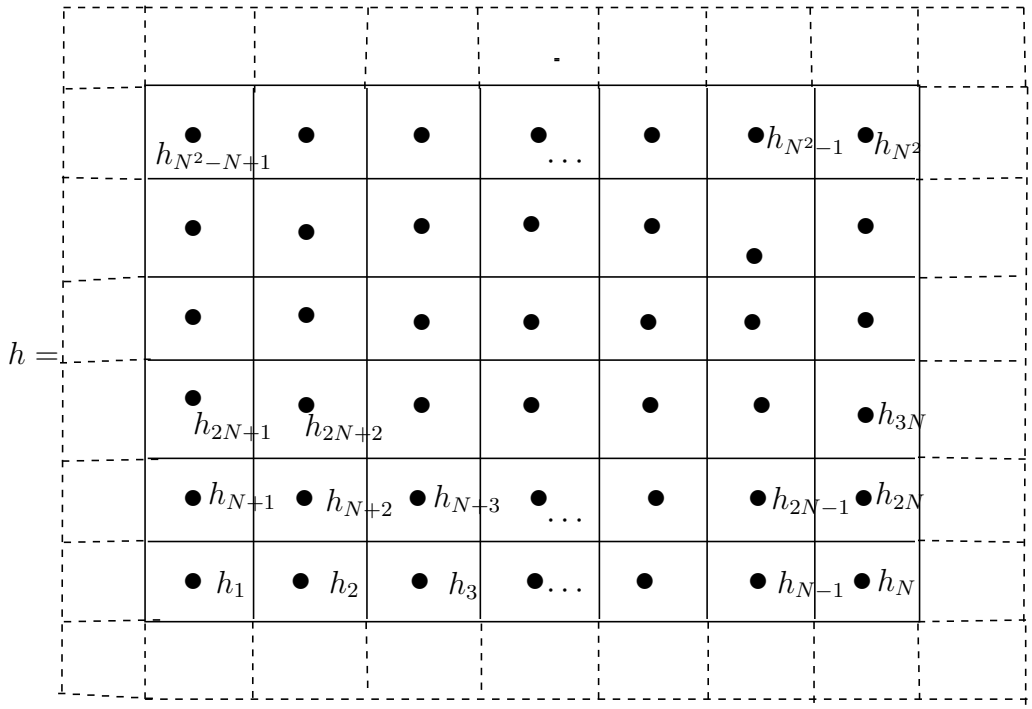

Figure 4.7: Numbering of the unknowns

For example when $N = 3$, equation (4.54) in matrix format gives the following matrix of coefficients:

$$\mathbf{A} = \begin{pmatrix} -(2+M) & 1 & 0 & 1 & 0 & 0 & 0 & 0 & 0 \\ 1 & -(3+M) & 1 & 0 & 1 & 0 & 0 & 0 & 0 \\ 0 & 1 & -(4+M) & 0 & 0 & 1 & 0 & 0 & 0 \\ 1 & 0 & 0 & -(3+M) & 1 & 0 & 1 & 0 & 0 \\ 0 & 1 & 0 & 1 & -(4+M) & 1 & 0 & 1 & 0 \\ 0 & 0 & 1 & 0 & 1 & -(5+M) & 0 & 0 & 1 \\ 0 & 0 & 0 & 1 & 0 & 0 & -(4+M) & 1 & 0 \\ 0 & 0 & 0 & 0 & 1 & 0 & 1 & -(5+M) & 1 \\ 0 & 0 & 0 & 0 & 0 & 1 & 0 & 1 & -(6+M) \end{pmatrix}.$$

The solution vector $\mathbf{h}$ is given by

$$\mathbf{h} = \begin{pmatrix} h_1 = h_{1,1} \\ h_2 = h_{2,1} \\ h_3 = h_{3,1} \\ h_4 = h_{1,2} \\ h_5 = h_{2,2} \\ h_6 = h_{3,2} \\ h_7 = h_{1,3} \\ h_8 = h_{2,3} \\ h_9 = h_{3,3} \end{pmatrix}_{k+1} \tag{4.55}$$

and the right hand side vector $\mathbf{b}$ is given by

$$\mathbf{b} = -M \begin{pmatrix} h_1 \\ h_2 \\ h_3 \\ h_4 \\ h_5 \\ h_6 \\ h_7 \\ h_8 \\ h_9 \end{pmatrix}_k - \begin{pmatrix} 0 \\ 0 \\ 24 \\ 0 \\ 0 \\ 24 \\ 24 \\ 24 \\ 48 \end{pmatrix} \tag{4.56}$$

where k and $k+1$ are time levels.

The value of the parameters $\Delta x, \Delta t, S$ and T are known as is the value of the hydraulic head, $h_{i,j}^k$. The set of equations must be solved simultaneously at each time step, starting from a set of initial conditions where $h_{i,j}$ is known for all (i, j) and proceeding through the time steps, $k = 1, 2, 3, \ldots$.

Chapter 5

Results and Discussion

5.1 Introduction

To generate the results presented in this Chapter, a Matlab code was written and a simulation of model (4.33) was carried out. The results from the simulations are presented in the following Sections. The Matlab code for the simulations is given in Appendix A.

5.2 Dirichlet and Homogeneous Neumann Boundary Conditions

When we specify the head at the northern and eastern borders to be 12m and make the western and southern borders impermeable as shown in Figure 5.1, we obtain the results presented in Figures 5.2 to 5.9.

The variation of hydraulic head with time at selected points in the domain is shown in Figure 5.2. The groundwater level in the aquifer rises due to the inflow from the northern and eastern borders and after about 500 days, the water level stays constant at 12m above the aquifer bottom.

The direction of flow after 100 days and after 1000 days at selected points in the domain is shown in Figures 5.3 and 5.4. Inflow is through the northern and eastern boundaries. The arrow lines point in the direction of groundwater flow and the magnitude of flow is indicated by the arrow length. Figure 5.2 also shows that the nearer a point is to the northern and eastern inflow borders the faster the water level at the point gets to the Dirichlet value of

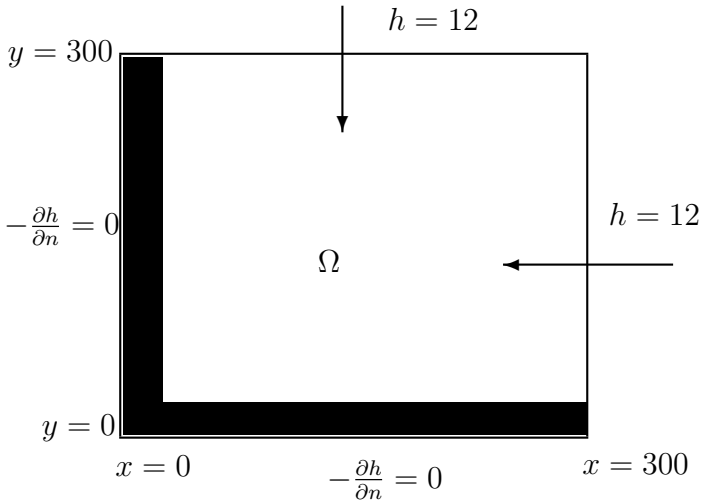

Figure 5.1: Dirichlet and Homogeneous Neumann boundary conditions

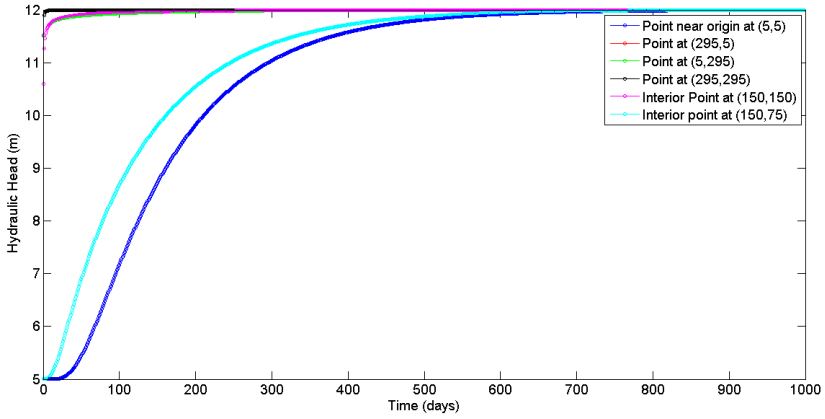

Figure 5.2: Variation of hydraulic head with time starting with an initial condition of $h(x, y, 0) = 5.0$

12m.

The groundwater head distribution is shown in Figure 5.5. The water head distribution after 500 days is approximately constant at 12m as shown by the same colour distribution.

When we start with an initial condition of $h(x, y, 0) = 15$m, in which the water level in the aquifer is way above the Dirichlet h value at the eastern and northern boundaries, groundwater flows out of the eastern and northern borders as shown in Figures 5.6 and 5.7. The outflow continues until the water level is equal to the head boundary condition at the eastern and northern borders as shown in Figure 5.8.

The groundwater head variation with time for selected points in the domain is shown in

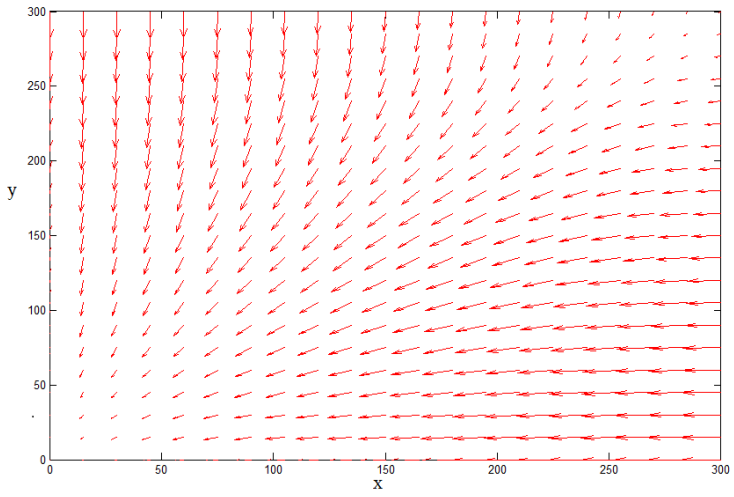

Figure 5.3: Groundwater flow direction after 100 days when initial condition is $h(x, y, 0) = 5.0$m.

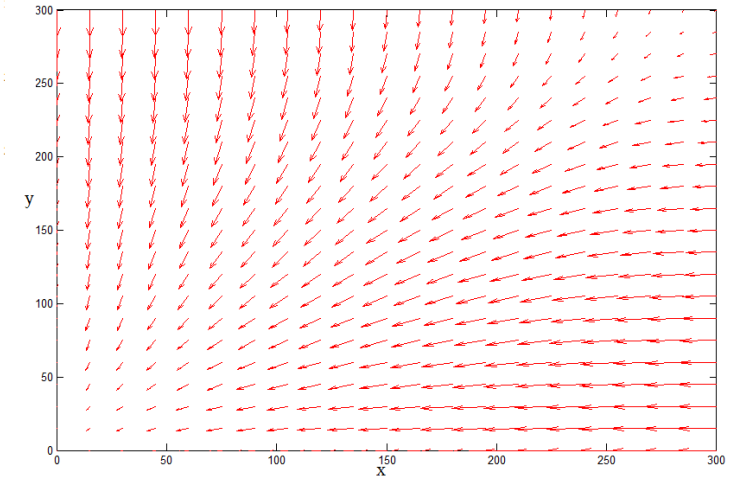

Figure 5.4: Groundwater flow direction after 1000 days when initial condition is $h(x, y, 0) = 5.0$m.

Figure 5.8. It should also be noted from Figure 5.8 that h again almost attained a steady state at about $t = 600$ days. The head distribution is shown in Figure 5.9.

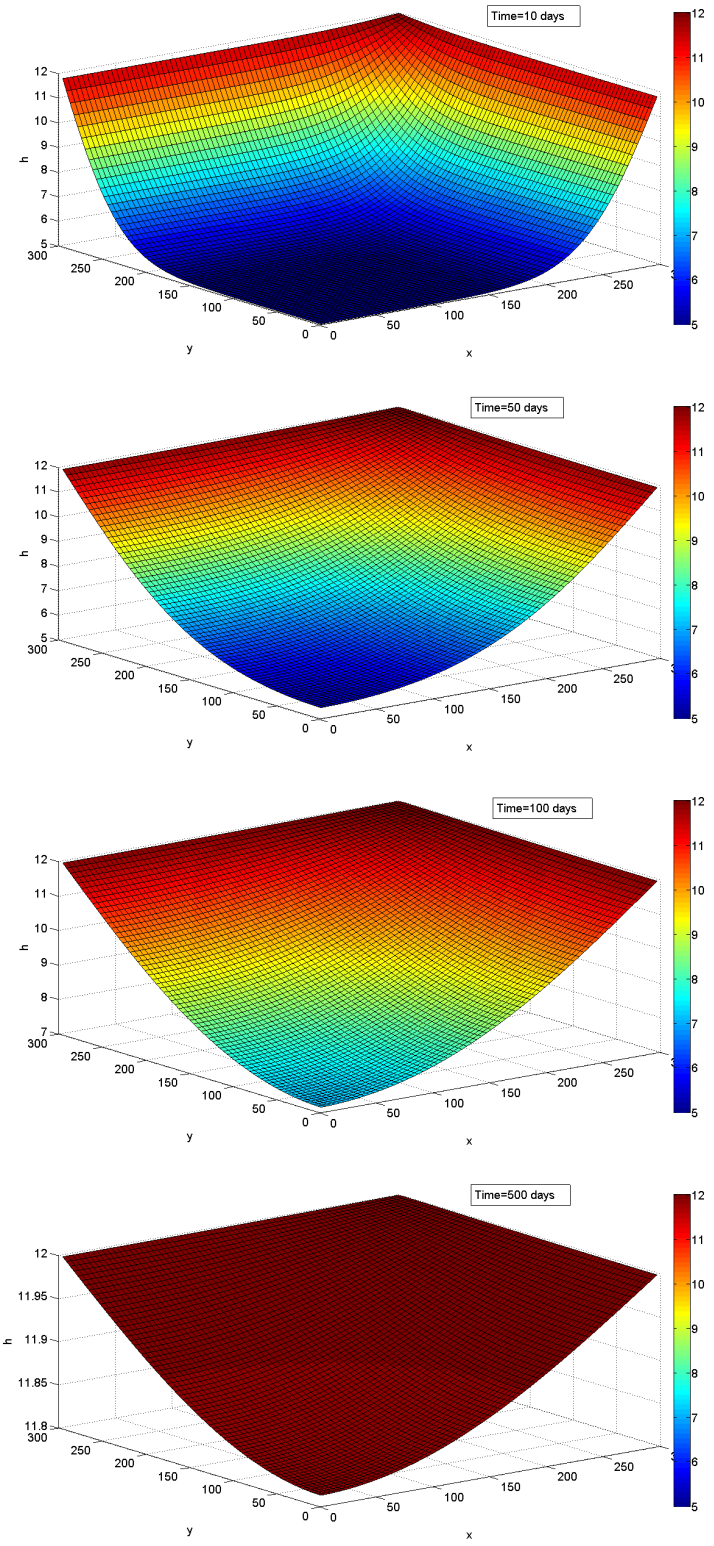

Figure 5.5: Groundwater head distribution starting with $h(x, y, 0) = 5.0$ at different times.

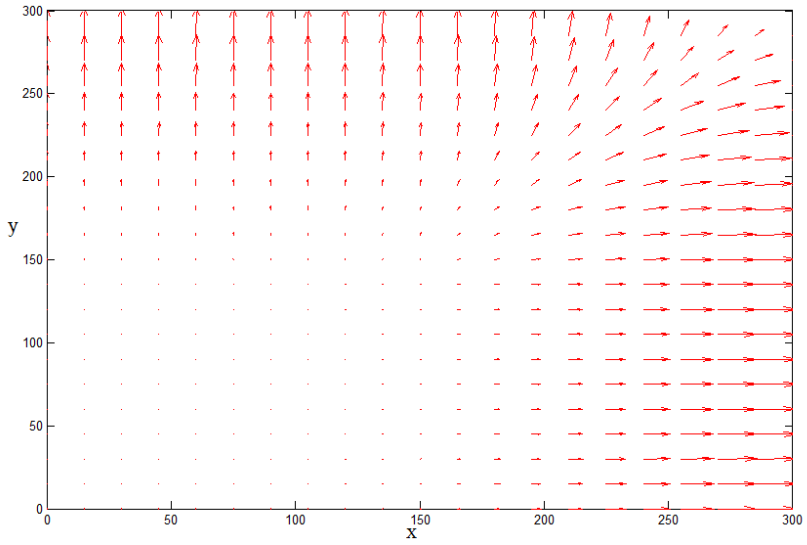

Figure 5.6: Groundwater flow direction after 10 days when initial condition is $h(x, y, 0) = 15.0$m.

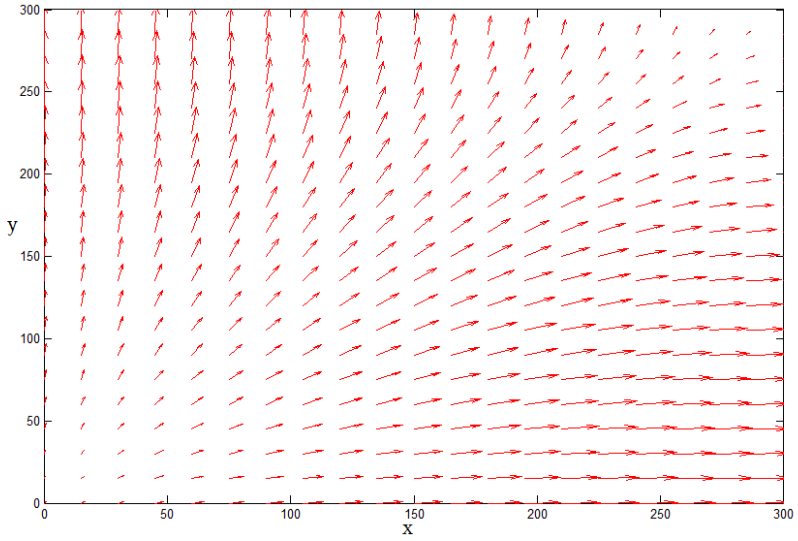

Figure 5.7: Groundwater flow direction after 100 days when initial condition is $h(x, y, 0) = 15.0$m.

5.3 Dirichlet and Non-Homogeneous Neumann Boundary Conditions

5.3.1 Outflow of 10.0m^3/day at the Western and Southern Borders

If we start with $h(x, y, 0) = 5.0$m and allow an outflow of 10.0m^3/day ($1.157 \times 10^{-4}\text{m}^3$/s) at the western and southern borders as shown in Figure 5.10, the variation of hydraulic head

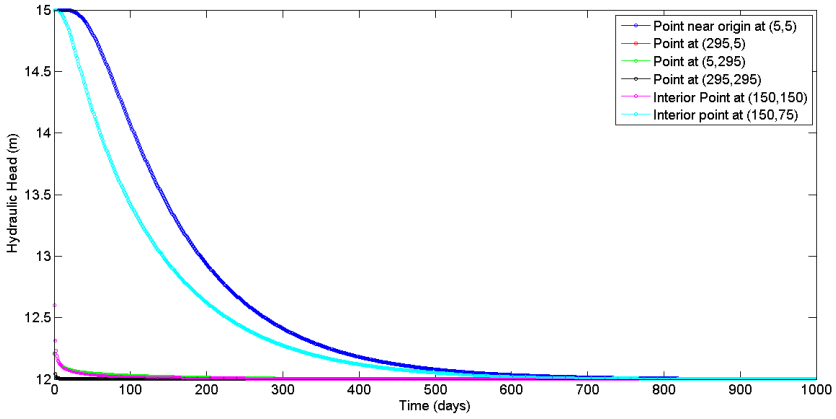

Figure 5.8: Variation of hydraulic head with time starting with an initial condition $h(x, y, 0) = 15.0$.

with time at selected points in the domain is shown in Figure 5.11.

As in the case when the western and southern boundaries were impermeable, groundwater rises in the aquifer and, after 600 days, approaches the head boundary condition at the eastern and northern borders and almost stays constant afterwards.

The direction of flow is shown in Figures 5.12 and 5.13. The head distribution is shown in Figure 5.14. The groundwater level at 500 and 1000 days is almost constant at 12m as shown by the same colour distribution.

If we start with an initial condition of $h(x, y, 0) = 15$m, which is way above the specified head boundary condition at the eastern and northern boundaries, there is too much water in the aquifer and groundwater flows out of the system through the northern and eastern boundaries as shown in Figure 5.15, which would have been inflow borders. It reduces till it reaches 12m and stays constant as shown in Figure 5.16. After the water level in the system is at the 12 m specified head value at the Dirichlet boundary, the eastern and northern borders act as inflow boundaries while the western and southern borders act as outflow boundaries as shown in Figure 5.17. The head distribution at different times is shown in Figure 5.18.

5.3.2 Outflow of 50.0m^3/day at the Western and Southern Borders

If we increase the outflow through the western and southern borders from 10.0 to 50.0 m^3/day and starting with $h(x, y, 0) = 5.0$m, the water level in the aquifer rises and approaches a steady value as shown in Figure 5.19 at selected points in the aquifer. We observe that the closer a point is to the northern and eastern inflow boundaries, the faster the water level

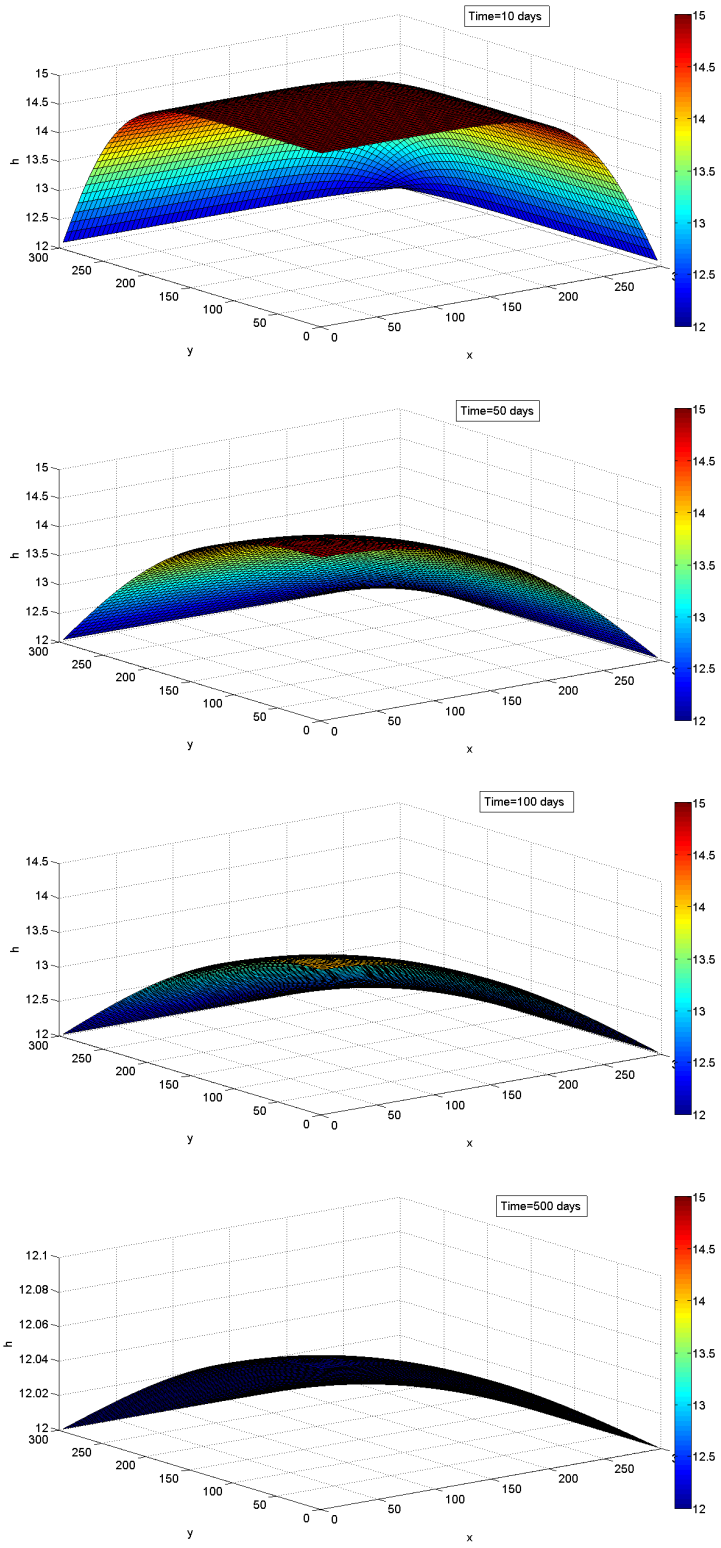

Figure 5.9: Groundwater head distribution starting with $h(x, y, 0) = 15.0$ at different times.

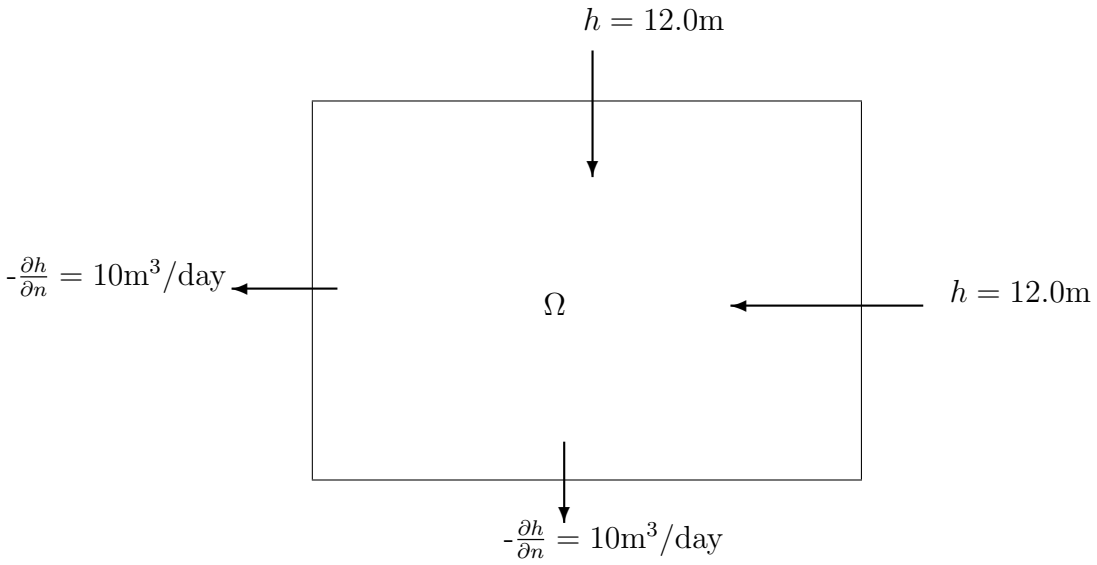

Figure 5.10: Dirichlet and non-homogeneous Neumann boundary conditions of $10.0\text{m}^3/\text{day}$.

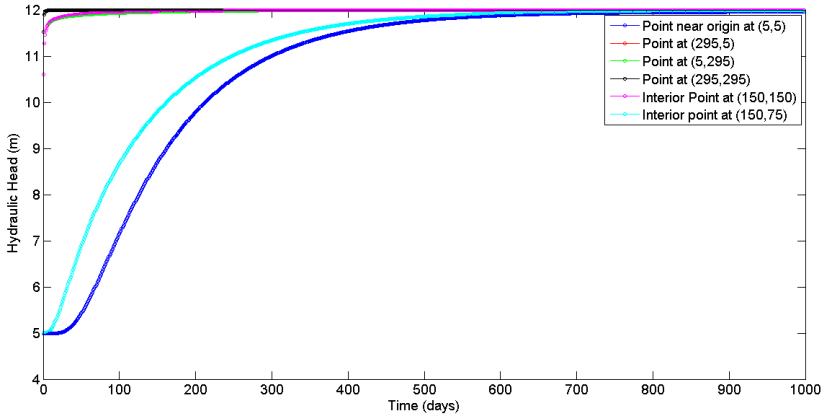

Figure 5.11: Variation of hydraulic head with time starting with an initial condition of $h(x, y, 0) = 5.0\text{m}$ and having a Neumann boundary condition $-\dfrac{\partial h}{\partial \mathbf{n}} = 10.0\text{m}^3/\text{day}$ at the western and southern borders.

at the point rises and attains the steady state. We also note that the water level at some points in the aquifer does not necessarily rise to 12m due to the outflow at the southern and western borders. The closer a point in the aquifer is to the outflow borders, the lower its water level is below 12m at the steady state.

The direction of flow after 100 and 1000 days is shown in Figures 5.20 and 5.21. The groundwater head distribution is shown in Figure 5.22.

If we start with an initial condition of $h(x, y, 0) = 15\text{m}$, which is way above the values of h at the eastern and northern boundaries, there is too much water in the aquifer and groundwater

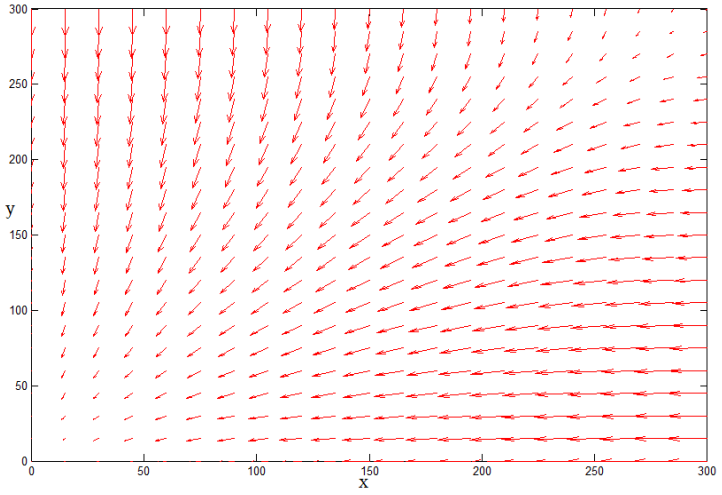

Figure 5.12: Groundwater flow direction after 100 days when initial condition is $h(x, y, 0) = 5.0$m.

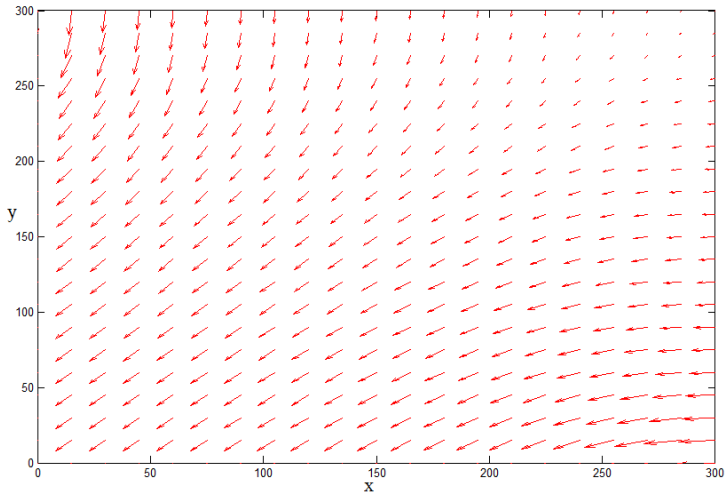

Figure 5.13: Groundwater flow direction after 1000 days when initial condition is $h(x, y, 0) = 5.0$m.

flows out of the system through the would be inflow northern and eastern borders, as shown in Figure 5.23, until a steady state is obtained, as shown in Figure 5.24.

After the water in the system is below the 12m specified head, the eastern and northern borders act as inflow boundaries while the western and southern borders act as outflow boundaries as shown in Figure 5.25. The groundwater head distribution is shown in Figure 5.26.

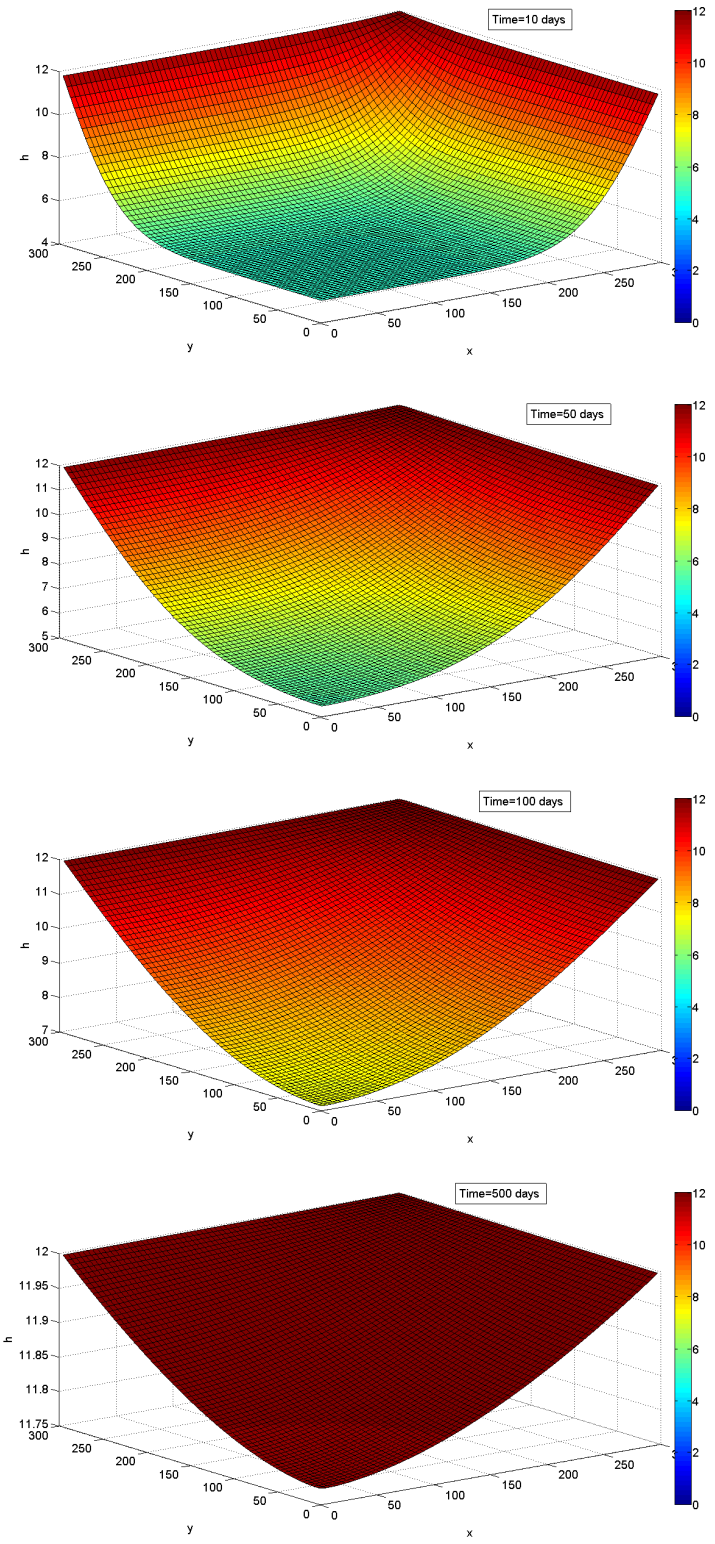

Figure 5.14: Groundwater head distribution starting with $h(x, y, 0) = 5.0\text{m}$ and having a Neumann boundary condition $-\dfrac{\partial h}{\partial \mathbf{n}} = 10.0\text{m}^3/\text{day}$ at the western and southern borders.

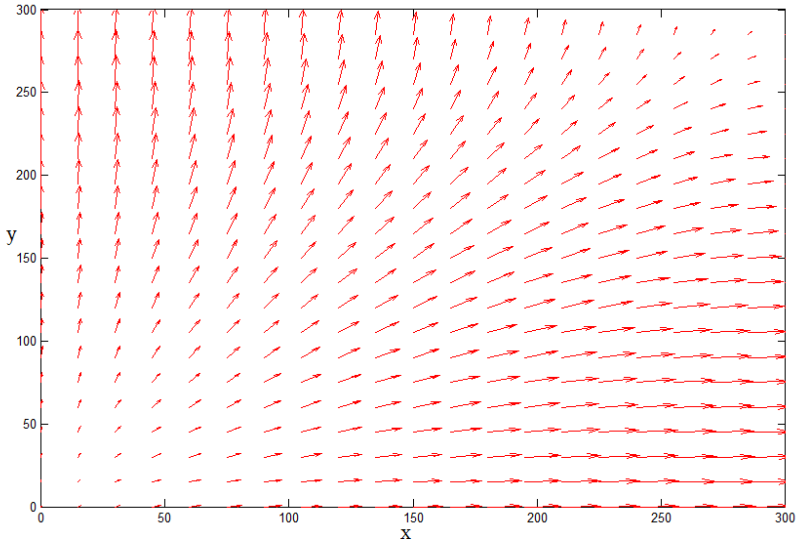

Figure 5.15: Groundwater flow direction after 100 days when initial condition is $h(x, y, 0) = 15.0$m.

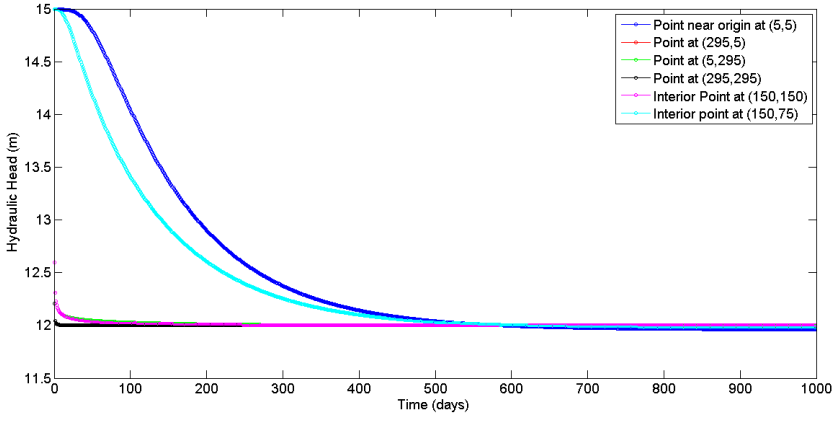

Figure 5.16: Variation of hydraulic head with time starting with an initial condition of $h(x, y, 0) = 15.0$m and having a Neumann boundary condition $-\dfrac{\partial h}{\partial \mathbf{n}} = 10.0\text{m}^3/\text{day}$ at the western and southern borders.

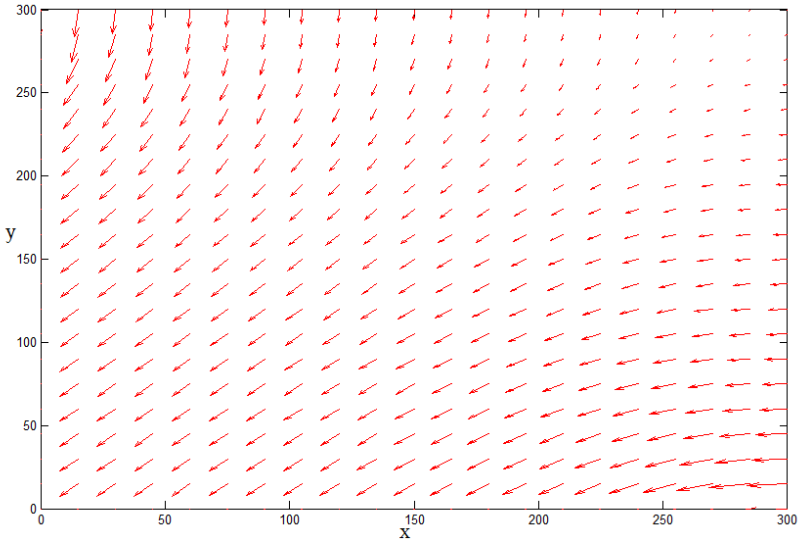

Figure 5.17: Groundwater flow direction after 1000 days when initial condition is $h(x, y, 0) = 5.0$m.

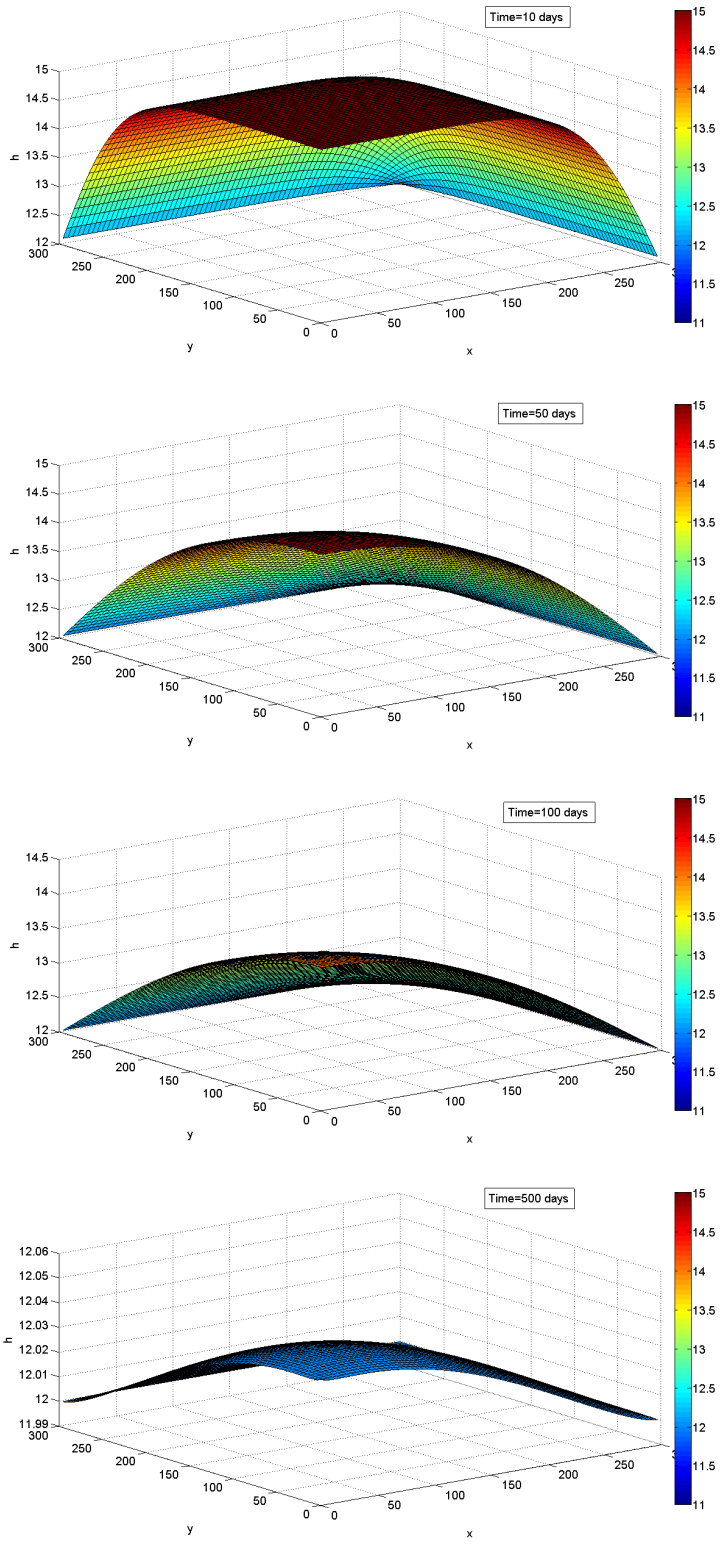

Figure 5.18: Groundwater head distribution at different times starting with $h(x, y, 0) = 15.0$m and having a Neumann boundary condition $-\dfrac{\partial h}{\partial \mathbf{n}} = 10.0\text{m}^3/\text{day}$ at the western and southern borders.

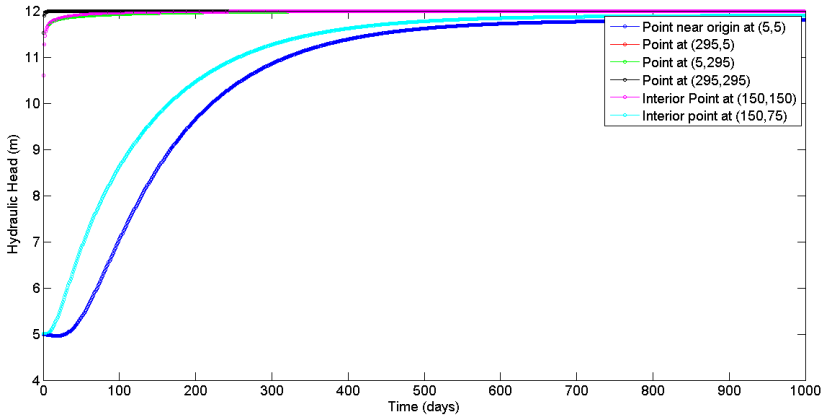

Figure 5.19: Variation of hydraulic head with time starting with an initial condition of $h(x, y, 0) = 5.0\text{m}$ and having a Neumann boundary condition $-\dfrac{\partial h}{\partial \mathbf{n}} = 50.0\text{m}^3/\text{day}$ at the western and southern borders.

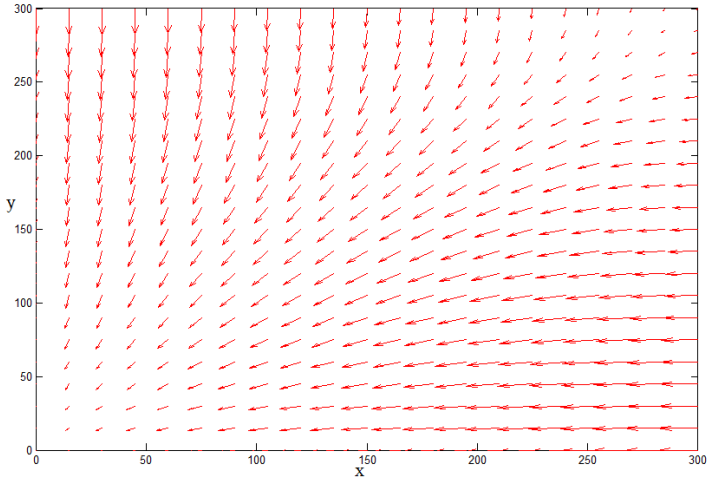

Figure 5.20: Groundwater flow direction after 100 days when initial condition is $h(x, y, 0) = 5.0\text{m}$.

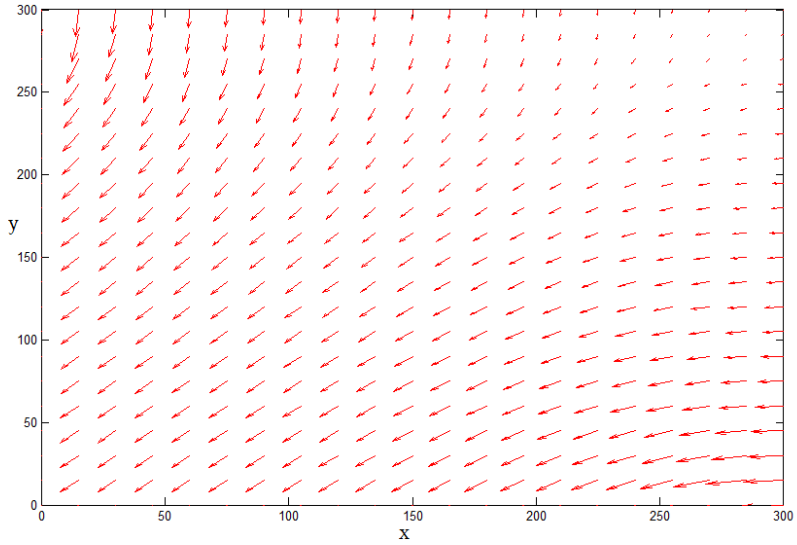

Figure 5.21: Groundwater flow direction after 1000 days when initial condition is $h(0, x, y) = 5.0$m.

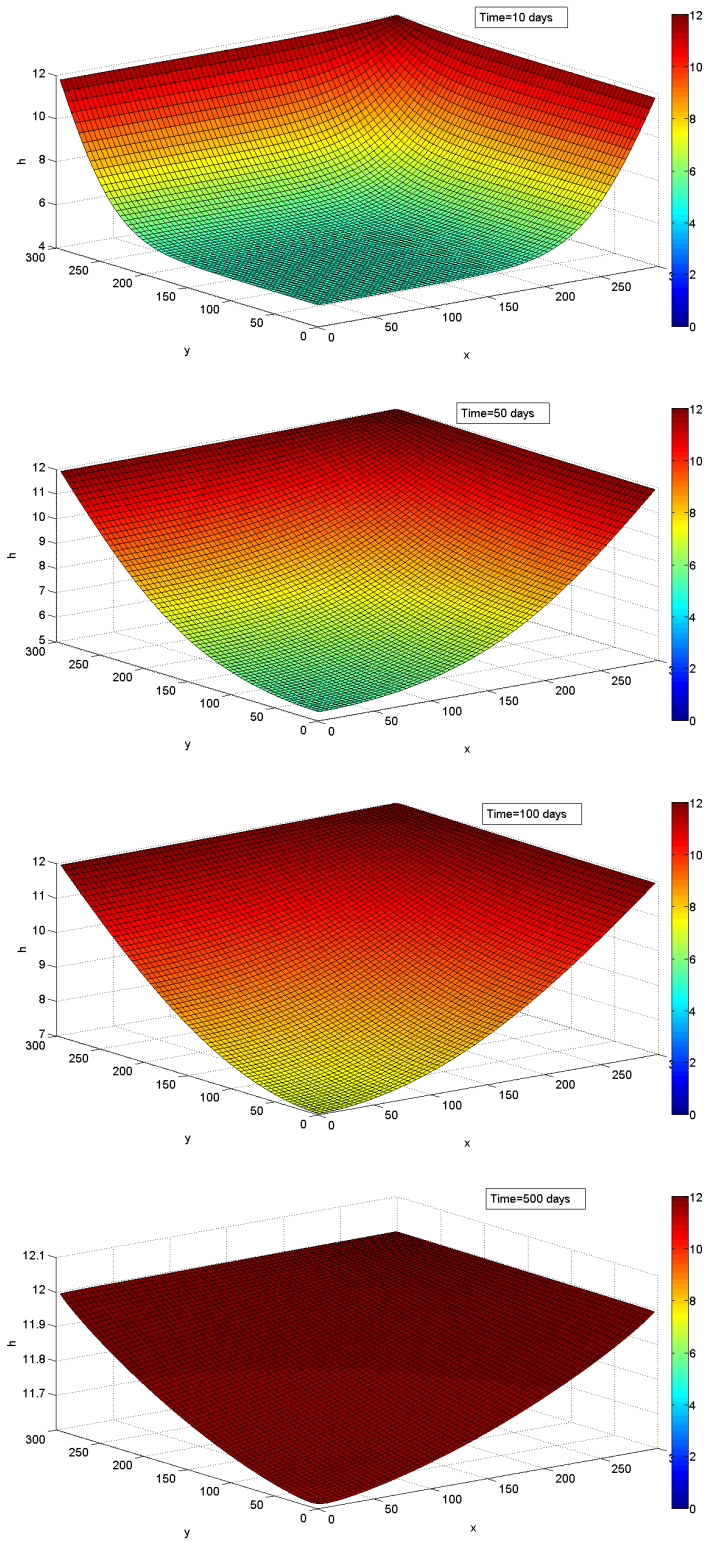

Figure 5.22: Groundwater head distribution at different times starting with $h(0, x, y) = 5.0\text{m}$ and having a Neumann boundary condition $-\dfrac{\partial h}{\partial \mathbf{n}} = 50.0\text{m}^3/\text{day}$ at the western and southern borders.

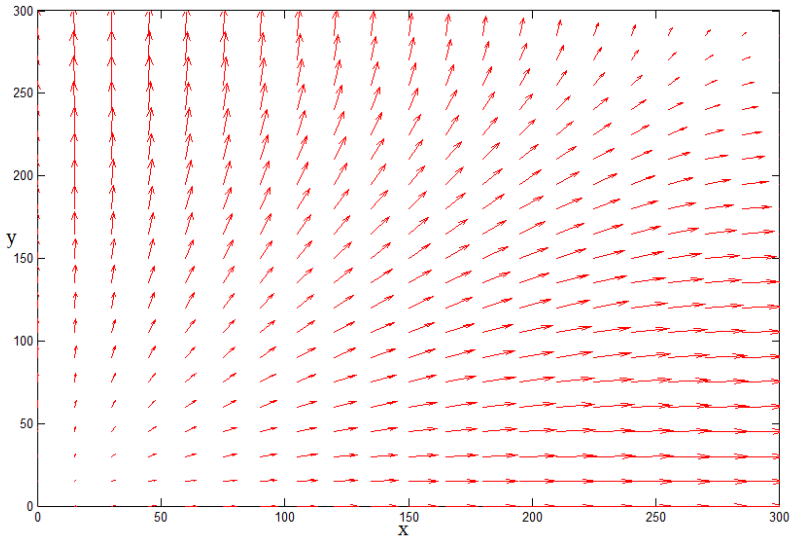

Figure 5.23: Groundwater flow direction after 100 days when initial condition is $h(0, x, y) = 15.0$m.

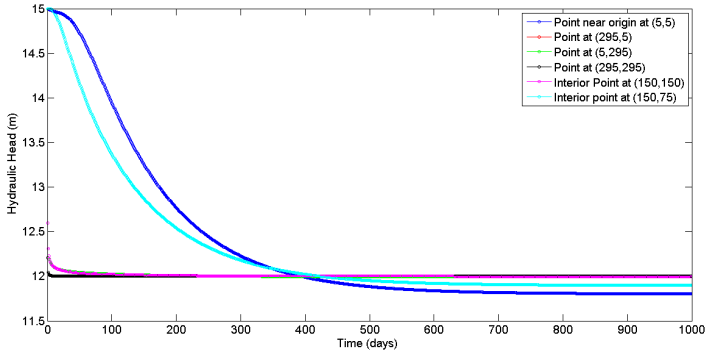

Figure 5.24: Variation of hydraulic head with time starting with an initial condition of $h(x, y, 0) = 15.0$m and having a Neumann boundary condition $-\dfrac{\partial h}{\partial \mathbf{n}} = 50.0\text{m}^3/\text{day}$ at the western and southern borders.

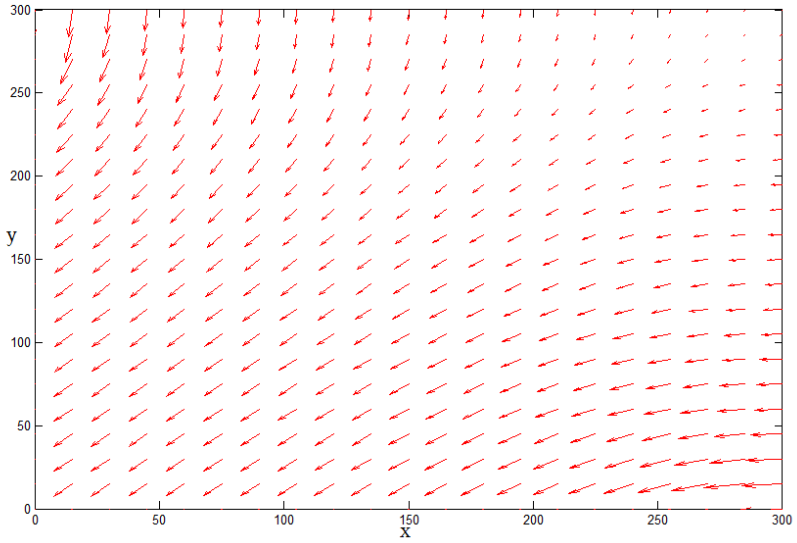

Figure 5.25: Groundwater flow direction after 1000 days when initial condition was $h(x, y, 0) = 15.0\text{m}$.

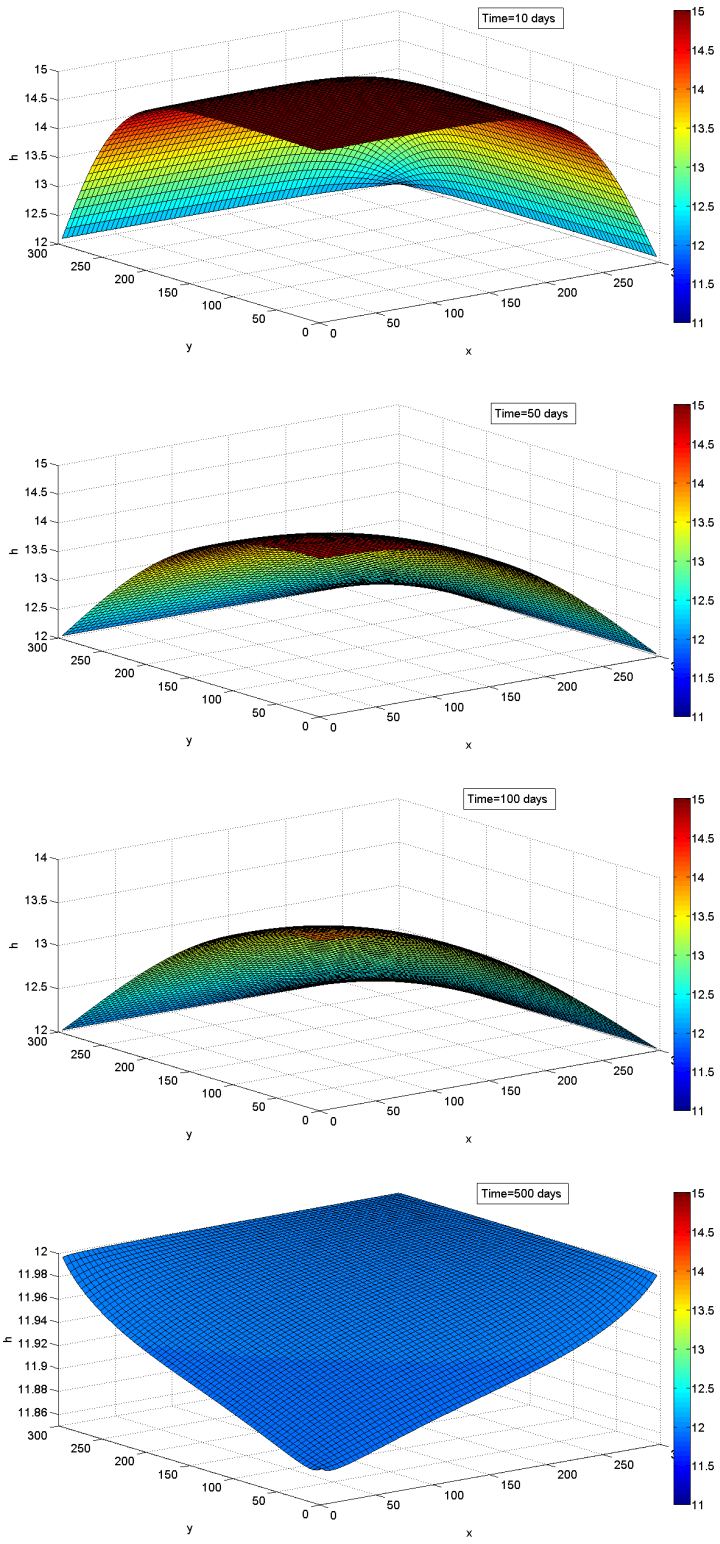

Figure 5.26: Groundwater head distribution at different times starting with $h(x, y, 0) = 15.0$m and having a Neumann boundary condition $-\dfrac{\partial h}{\partial \mathbf{n}} = 50.0\text{m}^3/\text{day}$ at the western and southern borders.

Chapter 6

Conclusions and Recommendations

6.1 Introduction

In this chapter, we state the conclusions that are derived from the results presented in the previous chapter and also make recommendations for future work.

6.2 Conclusions

An orthogonal grid finite volume scheme applied to an isotropic transient groundwater flow model has been described in this work. We have used quadrilateral control volumes with nodes at the centers of the control volume and assumed that h varies linearly between any two nodal points. We have also seen that in the FVM scheme, conservation is guaranteed for each cell, and this ensures that both local and global conservation are guaranteed no matter how coarse the mesh. A fully implicit scheme has been used to approximate the derivatives. The spatial truncation error is $O((\Delta x)^2)$ and the temporal truncation error is $O(\Delta t)$, that is, the fully implicit scheme is second order accurate in space and first-order accurate in time. The scheme is also unconditionally stable. We have used direct methods to solve the discretized system.

From the results presented in Chapter 5, we observed that when the outflow boundaries were impermeable and we started the simulation with the water level in the aquifer less than the prescribed h at the inflow eastern and northern borders, water would enter the aquifer and accumulate until the level is equal to the fixed Dirichlet h value at the inflow borders. After this, the water level would remain constant at $h = 12$m implying that the same amount of

water that comes into the aquifer would also get out through the same inflow borders.

When the initial water level in the system is much higher than the fixed h value at the Dirichlet borders, water would use the inflow borders to move out of the system until a steady state is reached where the water level is constant at $h = 12$m. Thus the wouldbe inflow boundaries would also act as outflow borders depending on the amount of water in the aquifer.

When we allowed outflow from the western and southern boundaries which were previously impermeable, the results were almost the same as those for the impermeable boundaries. Water either accumulates in or leaves the system until it reaches a steady head value. The difference was that in the case where we allowed outflow, the steady value could be less that the fixed Dirichlet head value at the inflow boundaries. The steady state for each point in the aquifer depends on how much water is flowing out of the system compared to what is coming into the system and how far a point is from the inflow and outflow borders. Points nearer the outflow borders tend to have a lower steady head value than those farther away and closer to the inflow borders. This is due to the fact that the points nearer the inflow boundaries receive water earlier and more often than points farther away from the inflow borders. Also, the specified head boundaries guarantee that the water level in the system cannot be above Dirichlet head boundaries.

6.3 Recommendations

In this work, we assumed that the study area was isotropic which in reality is not the case. We also assumed a fixed h value at the inflow borders which in nature is almost impossible. The inflow into the study area depends on whether its rainy season or dry season and there are always variations in the inflow of water depending on the season of the year. Further research would focus on using an anisotropic model and also using time dependent boundary conditions. An error analysis of our model would also be interesting to look at in future work.

References

Barrash, W., & Dougherty, M. E. (1997). Modelling axially symmetric and nonsymmetric flow to a well with modflow, and application to goddard2 well test , boise, idaho. *Groundwater*, *35*(4), 602-611.

Batu, V. (2006). *Applied flow and solute transport modeling in aquifers: Fundamental principles and analytical and numerical methods.* Taylor and Francis Group.

Bear, J. (1972). *Dynamics of fluids in porous media.* American Elsevier Publishing Company, Inc.

Bear, J., & Cheng, A. H. (2010). *Modeling groundwater flow and contaminant transport.* Springer.

Causon, D. M., Mingham, C. G., & Qian, L. (2011). *Introductory finite volume methods for pdes.* Ventus Publishing ApS.

Chapman, D. (1996). *Water quality assessments: A guide to the use of biodata, sediments and water in enviromental monitoring.* Taylor and Francis Group.

Clough, R. W. (1960, september). The finite element method in plane stress analysis. In *2nd conference on electronic computation.* New York: American Society of Civil Engineering.

Connor, J. J., & Brebbia, C. A. (1976). *Finite element techniques for fluid flow.* Butterworth and Co. Ltd.

Delleur, J. W. (1999). *The handbook of groundwater engineering.* CRC Press LLC.

Donea, J., & Huerta, A. (2003). *Finite element methods for flow problems.* John Wiley and Sons Ltd.

Faust, C. R., & Mercer, J. W. (1980). Groundwater modeling: Numerical models. *Groundwater*, *18*(4), 395-409.

Fitts, C. R. (2002). *Groundwater science.* Academic Press.

Freeze, R. A. (1971). Influence of the unsaturated flow domain on seepage through earth dams. *Water Resources Research*, *7*(4), 929-941.

Freeze, R. A. (1994). Henry darcy and the fountains of dijon. *Ground Water*, *32*(1), 23-30.

Freeze, R. A., & Cherry, J. A. (1979). *Groundwater*. Prentince-Hall, Inc.

Freeze, R. A., & Witherspoon, P. A. (1966). Theoretical analysis of regional groundwater flow: Analytical and numerical solutions to the mathematical model. *Water Resources Research*, *2*(4), 641-656.

Gorelick, S. M., Freeze, R. A., Donohue, D., & Keely, J. F. (1993). *Groundwater contamination: Optimal capture and containment*. Lewis Publishers.

Herzog, A. (2007). *Transient groundwater modelling in peri-urban kampala, uganda*. TRITA-LWR Master Thesis.

Igboekwe, M. U., & Achi, N. J. (2011). Finite difference method of modelling groundwater flow. *Journal of Water Resource and Protection*, 192-198.

Iraj, J., & Witherspoon, P. A. (1968). Application of the finite element method to transient flow in porous media. *SPE journal*, *8*(3), 241-252.

Istok, J. (1989). *Groundwater modeling by the finite element method*. American Geophysical Union.

Jayantha, P. A., & W.Turner, I. (2001). A comparison of gradient approximations for use in finite volume computational models for two dimensional diffusion equations. *Numerical Heat Transfer, Part B*, *40*(5), 367-390.

Jayantha, P. A., & W.Turner, I. (2003). A second order finite volume technique for simulating transport in anisotropic media. *International Journal of Numerical Methods for Heat and Fluid Flow*, *13*(1), 31-56.

Kellogg, O. D. (1929). *Foundations of potential theory*. Springer Verlag.

König, L. F., & Weiss, J. L. (2009). *Groundwater :modelling, management and contamination*. Nova Science Publishers, Inc.

Kulabako, R. (2005). Analysis of the impact of anthropogenic pollution on shallow groundwater in peri-urban kampala. *TRITA-LWR LIC Thesis*.

Lehn O. Franke, T. E. R., & Bennett, G. D. (1984). *Definition of boundary and initial conditions in the analysis of saturated groundwater flow systems*.

Leveque, R. J. (2002). *Finite-volume methods for hyperbolic problems*. Cambbridge University Press.

Ligget, J. A., & Liu, P. L. F. (1983). *The boundary integral equation method for porous media flow*. Unwin Hyman.

Logan, D. L. (2007). *A first course in the finite element method*. Nelson.

Loudyi, D., Falconer, R. A., & Lin, B. (2007). Mathematical development and verification of a non-orthogonal finite volume model for groundwater flow applications. *Advances in Water Resources*, *30*(1), 29-42.

McDonald, M. G., & Harbaugh, A. W. (1988). A modular three-dimensional finite-difference

ground-water flow model. *Techniques of Water-Resource Investigation*, Book 6, Chap. A1.

McWhorter, D. B., & Sunada, D. K. (1977). *Groundwater hydrology and hydraulics*. Water Resources Publications.

Nelson, R. W. (1968). In place determination of permeability distribution distribution for heterogeneous porous media, through analysis of energy dissipation. *SPE Journal*, *8*(1), 33-42.

Patankar, S. V. (1980). *Numerical heat transfer and fluid flow*.

Pinder, G. F., & Bredehoeft, J. D. (1968). Applications of the digital computer for aquifer evaluation. *Water Resources Research*, *4*(5), 192-198.

Pinder, G. F., & Celia, M. A. (2006). *Subsurface hydrology*. John Wiley and Sons.

Prickett, T. A., & Lonnquist, C. G. (1971). *Selected digital computer techniques for groundwater resource evaluation*. Illinois State Water Survey.

Reeves, M., & Duguid, J. O. (1975). Water movement through saturated-unsaturated porous media: A finite-element galerkin model. *Rep. ORNL-4927, Oak Ridge National Laboratory, Oak Ridge, Tenn.*, 232 pp.

Remson, I., Appel, C. A., & Webster, R. A. (1965). Ground-water models solved by a digital computer. *Journal of the Hydraulics Division, ASCE*, *91*, 133-147.

Rozon, B. J. (1989). A generalized finite volume discretization method for reservoir simulation. *SPE Symposium on Reservoir Simulation, 6-8 February 1989, Houston, Texas*.

Rukia, H., Ejobi, F., & Kabagambe, E. K. (2005). The quality of water from protected springs in katwe and kisenyi parishes, kampala city, uganda. *African Health Sciences*, *5*(1), 14-20.

Schäfer, M. (2006). *Computational engineering : Introduction to numerical methods*. Springer-Verlag.

Spellman, F. R., & Whiting, N. E. (2004). *Enviromental engineer's mathematics handbook*. CRC Press.

Strack, O. D. L. (1989). *Groundwater mechanics*. Prentice Hall.

Thunvik, R. (2010). *Bwaise iii data sheet*. `http://www.kth.se/polopoly_fs/1.143493!/Menu/general/column-content/attachment/Bwaise%20III%20Data%20sheet.pdf`. ([Online; accessed 06-June-2013])

Trescott, P. C. (1975). Documentation of finite-difference model for simulation of three-dimensional groundwater flow. *U.S. Geological Survey Open-File Report 75-438*, 32 pp.

Trescott, P. C., & Larson, S. P. (1976). Documentation of finite-difference model for simulation of three-dimensional groundwater flow. *U.S. Geological Survey Open-File Report*

75-591, 21 pp.

Versteeg, H. K., & Malalasekera, W. (1995). *An introduction to computational fluid dynamics : The finite volume method*. Longman Scientific and Technical.

Wang, H. F., & Anderson, M. P. (1982). *Introduction to groundwater modeling: Finite difference and finite element methods*. W. H. Freeman and Company.

Yeh, G.-T., & Cheng, J.-R. (1994). *3dfemwater user manual: A three-dimensionalfinite-element model of water flow through saturated-unsaturated media*.

Zhang, Y. (2011). *Groundwater flow and solute transport modeling*. University of Myoming.

Appendix A

Matlab Code

```
clc;
close all;
clear all;
%physical parameters
L=300; % Length of aquifer (m)
W=300; % width of aquifer (m)
K=0.00399;
S=34.4205; % Storativity
T=0.05985; % Transmissivity
% Numerical Parameters
nx=70; % grid points in x-direction
ny=70; % grid points in y-direction
nt=1000; % number of time steps
dx = L/(nx); % Spacing of grid in x-direction
dy = W/(ny); % Spacing of grid in y-direction
dt=60*60*24 % time step in seconds (1 day)
u=dx/2:dx:L-dx/2;
v=dy/2:dy:W-dy/2;
[x,y] = meshgrid(u,v); % create grid
M=S*(dx)^(2)/(T*dt);
%Create the coefficient matrix
N=nx;
d=[-N,-1,0,1,N];
 v1=[ones(1,N^(2)-N),zeros(1,N)];
```

```
25  v21=ones(1,N*N-1);
26  for i=1:N-1
27      v21(i*N)=0;
28  end
29  v2=[v21,0];
30
31  v3=ones(1,N*N);
32  v3(1)=-(2+M);
33  v3(N*N)=-(6+M);
34  v3(N)=-(4+M);
35  v3(N*N-N+1)=-(4+M);
36  for i=2:N-1
37      v3(i)=-(3+M);
38      v3((i-1)*N+1)=-(3+M);
39      v3(N*N-N+i)=-(5+M);
40      v3(i*N)=-(5+M);
41  end
42 for i=1:N-2
43     for j=2:N-1
44         v3(i*N+j)=-(4+M);
45     end
46 end
47
48  v4=[0,v21];
49  v5=[zeros(1,N),ones(1,N^(2)-N)];
50
51  B=[v1',v2',v3',v4',v5'];
52  A=spdiags(B,d,N^(2),N^(2));
53
54 % right hand side vector:
55  b1=zeros(N*N,1);
56  b1(N*N)=48;
57  b1(1)=0.001157*dx;
58  b1(N)=24-0.0005787*dx;
59  b1(N*N-N+1)=24-0.0005787*dx;
60  for i=2:(N-1)
```

```
61        b1(i)=-0.0005787*dx  ;
62        b1(i*N)=24;
63        b1(N*N-N+i)=24;
64        b1((i-1)*N+1)=-0.0005787*dx;
65    end
66
67  % initial conditions
68    h=zeros(N*N,1);
69    for  i=1:N*N
70       h(i)=5;
71    end
72  %Compute solution vector
73  time=0;
74  %Frames = moviein(nt);
75  for  i=1:nt
76       b=-M*h-b1;
77       h_new=A\b;
78  %create 2D matrix from solution vector
79       H=vec2mat(h_new,N);
80       %[Hx,Hy]=gradient(H,dx,dy);
81       %Ddx=-Ddx; DDy=-Ddy;
82       surf(x,y,H);
83         caxis([0  12]);
84         colorbar;
85       %mesh(x,y,H);
86       %hold on;
87       %contour(u,u,H); hold on
88       %quiver(x,y,-Hx,-Hy)
89       %pcolor(x,y,H)
90       %MOVIE
91       %plot(time,h_new(155))
92       %hold on;
93  %       p1=plot(time,h_new(1),'marker','o','markersize',4);
94  %       hold on;
95  %       p2=plot(time,h_new(60),'r','marker','o','markersize',4);
96  %       p3=plot(time,h_new(3541),'g','marker','o','markersize',4);
```

```
97 %       p4=plot(time,h_new(3600),'k','marker','o','markersize',4);
98 %       p5=plot(time,h_new(1740),'m','marker','o','markersize',4);
99 %       p6=plot(time,h_new(870),'c','marker','o','markersize',4);
100      h=h_new;
101      time=time+1;
102    end
103  %legend([p1,p2,p3,p4,p5,p6],'Point near origin at (5,5) ','Point
       at (295,5)','Point at (5,295)','Point at (295,295)','Interior
       Point at (150,150)','Interior point at (150,75)');
```